

**DENDRIMER AND ACID FUNCTIONALIZED
MAGNETIC GRAPHENE OXIDE FOR LEAD (Pb)
REMOVAL FROM AQUEOUS SOLUTION**



**By
Muhammad Zakria
Registration No. 00000360457**

**Supervisor
Dr. Muhammad Arshad**

**A thesis submitted in partial fulfillment of the requirement for the
degree of Master of Science in Environmental Engineering**

**Institute of Environmental Sciences & Engineering
School of Civil & Environmental Engineering
National University of Sciences & Technology
Islamabad, Pakistan
2023**

APPROVAL CERTIFICATE

Certified that the contents and form of the thesis entitled


“Dendrimer and acid functionalized magnetic graphene oxide for lead (Pb) removal from aqueous solution.”

Submitted by


Mr. Muhammad Zakria

has been found satisfactory for partial fulfilment of the requirements of the degree of
Master of Science in Environmental Engineering.


Supervisor:


Dr. Muhammad Arshad
Professor
SCEE (IESE), NUST
NUST


Co-supervisor:


Dr. Hassan Anwer
Assistant Professor
SCEE (IESE),

GEC Member:


Dr. Aamir Alaud Din
Assistant Professor
SCEE (IESE), NUST

GEC Member:


Dr. Fouzia Perveen Malik
Professor
SINES, NUST

ACCEPTANCE CERTIFICATE

It is certified that the final copy of the MS Thesis written by Mr. Muhammad Zakria (Registration No: 00000360457) of SCEE (IESE) has been vetted by the undersigned, found complete in all respects as per NUST Statutes/ Regulations, is free of plagiarism, errors, and mistakes, and is accepted as partial fulfillment for the award of MS degree. It is further certified that necessary amendments as pointed out by GEC members of the scholar have also been incorporated in the said thesis.

Supervisor:

Prof. Dr. Muhammad Arshad

Dated: .. 25-01-2024

Dr. Muhammad Ali Inam
Assistant Professor
IESL (SCEE) NUST Islamabad

Head of Department: .. M Ali Inam

Dated: .. 29-01-2024

Prof. Dr. Imran Hashmi
Associate Dean
IESE (SCEE) NUST Islamabad

Associate Dean: .. Imran Hashmi

Dated: .. 29-01-2024

Principal & Dean SCEE: .. Dr. Muhammad Irfan ..
Principal & Dean
SCEE, NUST

Dated: .. 12 Feb, 2024

DECLARATION CERTIFICATE

I declare that this research work titled “**Dendrimer and acid functionalized magnetic graphene oxide for lead (Pb) removal from aqueous solution.**” is my own work. The work has not been presented elsewhere for assessment. The material that has been used from other sources has been properly acknowledged/referred.

Student Signature:

A handwritten signature in blue ink, appearing to read 'Zakria', is written over a dotted line. The signature is stylized and includes a horizontal line through the middle.

Muhammad Zakria

00000360457

PLAGIARISM CERTIFICATE

This thesis has been checked for plagiarism. The Turnitin report endorsed by the supervisor is attached.

Signature of Student:



Signature of Supervisor:



DEDICATION

I dedicate this thesis to my beloved parents who would always be a source of inspiration for me, always stood beside me, and brought me to this destination.

“O My Sustainer, bestow on my parents your mercy even as they cherished me in my childhood”.

ACKNOWLEDGEMENTS

Thanks to Allah Almighty, the "Most Kind" and "Most Merciful" Who blessed us with the aptitude, skills, and wisdom to accomplish this project. All respect to the Holy Prophet (P.B.U.H.) whose life is the model I am trying to base my life around.

I would like to thank my supervisor Dr. Muhammad Arshad for the privilege of starting my research career, his kind guidance, and valuable suggestions throughout my MS work. His support and motivation were a source of inspiration during the study. I also want to pay my utmost gratitude to my Co-supervisor Dr. Hassan Anwer (IESE) for his continuous support throughout my research work. I have gained invaluable experience in studies under his co-supervision. His time in the department discussion and specific ideas to improve the research work and thesis writing are very much appreciated.

I remain indebted to the guidance and committee members, Dr. Aamir Alaud Din (IESE) and Dr. Fouzia Perveen Malik (SINES) for taking time out of their busy schedules to attend progress reviews and giving helpful feedback and ideas about the research and thesis. My appreciation goes to the entire faculty, the staff of IESE, and all my classmates for their help and support during the research phase. I'm also grateful to my parents, family, and friends, for all the work they've done, the support they've given me, and the ideas they've given me to help me move forward in life.

Muhammad Zakria

TABLE OF CONTENTS

DEDICATION.....	vi
ACKNOWLEDGEMENTS	1
TABLE OF CONTENTS	2
LIST OF ABBREVIATIONS.....	5
LIST OF TABLES.....	6
LIST OF FIGURES.....	7
ABSTRACT	8
CHAPTER 1.....	9
INTRODUCTION.....	9
1.1. Water Pollution	9
1.2. Introduction to Lead	9
1.3. Nanotechnology.....	10
1.4. Graphene Oxide.....	10
1.5. Background of Dendrimers	11
1.6. Significance of the Research	12
1.7. Research Objectives	13
1.8. Aims of the Study	13
CHAPTER 2.....	14
LITERATURE REVIEW	14
2.1. Overview of Heavy Metal Contamination.....	14
2.2. Lead in Water.....	15
2.3. Health Impacts of Lead.....	15
2.4. Applications of Graphene based materials	17
2.4.1. Graphene based materials as Filtration	17
2.4.2. Graphene based materials as Photocatalysis	18
2.4.3. Graphene based materials as Adsorption	19
2.5. Synthesis of Nanoparticles	19
2.6. Lead Removal Technologies.....	20
2.6.1. Electrodialysis	20
2.6.2. Hydrogel.....	20
2.6.3. Photocatalytic process	21
2.6.4. Membrane filtration.....	21

2.6.5. Electrodeposition.....	22
2.6.6. Adsorption.....	22
CHAPTER 3.....	24
MATERIALS AND METHOD	24
3.1. Chemicals	24
3.2. Characterization Instruments	24
3.3. Methodology Overview	25
3.4. Synthesis of Graphene oxide	25
3.5. Synthesis of Magnetic Nano particles	26
3.6. Synthesis of Graphene oxide magnetic nano particles	26
3.7. Synthesis of Graphene oxide magnetic nano particles Dendrimers	26
3.8. Functionalization of citric, gallic, succinic and vanillic acid on GMNP...27	
CHAPTER 4.....	29
RESULTS AND DISCUSSION.....	29
4.1. Characterization.....	29
4.1.1. TEM Analysis.....	29
4.1.2. SEM Analysis.....	30
4.1.3. EDX Analysis.....	31
4.1.4. XRD Analysis.....	32
4.1.5. RAMAN Analysis	33
4.1.6. Functional groups identification.....	34
4.1.7. TGA Analysis	36
4.2. Performance Evaluation	37
4.2.1. Adsorption Studies	37
4.2.2. Performance Comparison.....	38
4.2.3. Zeta Potential.....	39
4.2.4. Effect of pH.....	40
4.2.5. Effect of Initial Solution Concentration	41
4.2.6. Study of Contact Time	42
4.2.7. Influence of Temperature	43
4.2.8. Isotherm Models.....	44
4.2.9. Kinetic Models	46
4.3. Regeneration.....	48
4.4. Contaminant Comparison with Literature Studies	49
CHAPTER 5.....	51

CONCLUSION AND RECOMMENDATIONS	51
5.1. Conclusion.....	51
5.2. Recommendations	52
REFERENCES.....	53

LIST OF ABBREVIATIONS

CA	Citric acid
DI	Distilled water
EDS	Energy dispersive spectroscopy
Fe ₃ O ₄	Iron oxide
FTIR	Fourier transmission infrared
GA	Gallic acid
GO	Graphene oxide
GMNP	Graphene oxide magnetic nano particles
MNP	Magnetic nano particle
Pb	Lead
PZC	Point of zero charge
SA	Succinic acid
SEM	Scanning electron microscope
TEM	Transmission electron microscope
TGA	Thermogravimetric analyzer
VA	Vanillic acid
XRD	X-Ray diffraction

LIST OF TABLES

Table 1: EDX of MNP, GMNP-40, and GMNP-CA.....	31
Table 2: Parameters of the isotherm models for the sorption of Pb.....	45
Table 3: Parameters of the kinetic models for the sorption of pb	47
Table 4: Comparing latest prepared nano composites' performance in removing Pb..	49

LIST OF FIGURES

Figure 1: Schematic diagram of the methodology	25
Figure 2: Schematic diagram of CA, SA, VA and GA functionalized GMNP synthetic procedure.....	28
Figure 3: TEM images of (a) GMNP-50, (b) GMNP-40, (c) GMNP-30, (d) GMNP-20, (e) GMNP-G1, (f) GMNP-VA, (g) GMNP-CA, and (h) GMNP-SA.....	30
Figure 4: SEM images of (a) MNP, (b) GMNP-40, and (c) GMNP-CA	31
Figure 5: XRD Graphite, GO, MNP, GMNP-20, GMNP-G1, and GMNP-VA.	33
Figure 6: Raman spectra of Graphite, GO, GMNP-20, GMNP-G1, and GMNP-VA..	34
Figure 7: FTIR spectra of Graphite, GO, MNP, GMNP-50, GMNP-40, GMNP-30, GMNP-20, GMNP-G1, GMNP-VA, GMNP-CA, GMNP-SA, and GMNP-GA.....	36
Figure 8: TGA analysis of GO, MNP, GMNP-50, GMNP-20, GMNP-G1, GMNP-VA, GMNP-CA, and GMNP-SA.	37
Figure 9: Removal Comparison of different composites (GO, MNP, GMNP-20, GMNP-30, GMNP-40, GMNP-50, GMNP-60, GMNP-70, GMNP-G1, GMNP-VA, GMNP-CA, GMNP-SA, and GMNP-GA)	39
Figure 10: Zeta potential of GMNP-40, GMNP-G1, GMNP-VA, GMNP-CA, GMNP-SA, and GMNP-GA	40
Figure 11: Effect of pH on Pb adsorption by GMNP-G1, GMNP-VA, GMNP-CA, GMNP-SA, and GMNP-GA	41
Figure 12: Effect of initial concentration for adsorption efficiency of GMNP-CA on Pb ions.....	42
Figure 13: Effect of contact time for adsorption efficiency of GMNP-CA on Pb ions	43
Figure 14: Effect of Temperature on Pb adsorption by GMNP-VA, GMNP-CA, GMNP-SA, and GMNP-GA	44
Figure 15: (a) Langmuir model and (b) Freundlich model for the adsorption of Pb ions on GMNP-CA	46
Figure 16: (a) pseudo first order and (b) pseudo second order for the adsorption of Pb ions on GMNP-CA	48
Figure 17: Regeneration of GMNP-CA for Pb adsorption	49

ABSTRACT

Synthesis and optimization of nano sorbents for lead (Pb) removal from water is challenging. In this study, graphene oxide (GO) was decorated with magnetic nanoparticles (MNPs) in various weight ratios (20%-70%). Polyamidoamine dendrimers were anchored on the GO-MNP composites to passivate MNP surface and generate amine-terminal groups on GO, which were functionalized with four different organic acids to construct cage-like structures for Pb removal from contaminated water. The composites were characterized using transmission electron microscope, scanning electron microscope, energy dispersive spectroscopy, X-ray diffraction, Raman spectroscopy, Fourier transform infrared, thermogravimetric, and zeta potential analysis. The Pb removal increased significantly with GO weight percentage up to 40% resulting in 51% Pb removal in 24 h. The organic acid functionalization improved the Pb removal by adsorption through electrostatic attraction, hydrogen bonding, and π - π interactions. Pb removal efficiency of citric acid (CA), gallic acid (GA), succinic acid (SA), and vanillic acid (VA) functionalized GO-MNP was 94%, 71%, 88%, and 66%, respectively. The highest removal efficiency of GO-MNP-CA was attributed to the linear structure of CA and the number of adsorptive sites per molecule. The monolayer adsorption hypothesis has been bolstered by the Langmuir model's superior fit to the Pb adsorption over the Freundlich model. GMNP-CA attained 23.5 mg/g adsorption capacity at an equilibrium adsorption time of 150 min with 100 mg/L dosage of adsorbent that possesses the ability due to the presence of tricarboxylic groups. GMNP-CA maintained 90% Pb adsorption in the tenth cycle of the reusability experiment which suggested to be best for practical application.

INTRODUCTION

1.1. Water Pollution

Aquatic pollution pertains to the conveyance of pollutants into fresh water, which brings down its quality and also has a bearing on the ecosystem (Heidari et al., 2023). This system includes the addition of dissolved and suspended solids, enduring hazardous contaminants such as chemical substances, pesticides, and heavy metals. Public recognition of water pollution and its negative effects has recently increased coordinated efforts to reduce pollution. For the reason of their hazardous effects and intake through the food chain, heavy metal pollution of water is a problem that affects all environmental aspects (Barkade et al., 2022; Krishna et al., 2023).

1.2. Introduction to Lead

Lead (Pb) is a heavy metal that is in period 6 and group IV of the periodic table of elements. Its atomic weight is 207.2, its melting and boiling points are 327.4 and 1725 °C, respectively, and its density is 11.4 g/cm³. Its atomic number is 82. It takes place physically; blue-gray metal that is typically found in minerals that are tainted with other elements like oxygen or sulphur. Currently, lead (II) is produced annually in the world in roughly 5.4 M tons of batteries (Wuana & Okieimen, 2011; Zahra, 2012).

Pb, renowned for its extreme toxicity, has emerged as a significant global environmental concern. Incidences of lead presence in drinking water have been documented in several cities within the United States. The WHO's and the US EPA's permissible limits for lead are 10 µg/L and 15 µg/L, respectively (Wang et al., 2020). Pb, a toxic heavy metal, is widespread free from mining, batteries, textiles, electroplating, dyeing, explosives, and other industries (Rashida & Abdul, 2020). A primary contributor to lead contamination in water to drink arises from involving lead components within water supply systems, like water lines, solders, and fixtures. The persistence of decade-old pipelines containing lead can result in lead concentrations reaching tens of milligrams per liter, especially following instances of human-induced mishandling or natural disasters. Prolonged contact with lead, even at minimal concentrations, leads to elevated blood lead levels due to its bio-accumulative nature. This poses a significant health risk,

particularly to the nervous system and brain, with heightened susceptibility observed in infants and children (Wang et al., 2020).

1.3. Nanotechnology

Recent advances in nanotechnology have led to significant impacts on various industries, such as manufacturing, healthcare, electronics, agriculture, renewable energy, and cosmetics, where the utilization of nanoparticles has seen substantial growth. Nanoparticles (NPs) are typically defined as materials or compounds that have a size range from 1 to 100 nm with a minimum of one dimension (Azadmanjiri et al., 2016). The NPs typically possess unique magnetic and optical properties and are superior to conventional materials due to their enhanced surface activity as well as heightened catalytic efficiency. These properties are linked to the increased surface area of NPs owing to their smaller size (Pabbati et al., 2021).

1.4. Graphene Oxide

Despite its relatively brief history, graphene has captivated significant attention across diverse fields, including environmental science, physics, materials science, chemistry, and biology. This surge in interest follows earlier studies on C60 fullerene and carbon nanotubes. Novoselov and his colleagues, in 2004, formally defined graphene as a two-dimensional honeycomb lattice made up of a flat monolayer of carbon atoms that have been closely arranged. Additionally, graphene is characterized as graphite with a layer number less than 10, dividing it into three groups: graphene with a single layer, two layers, and few layers (Rudrapati, 2020).

For graphitic materials in a variety of dimensionalities, graphene is a fundamental building component. When graphene is configured into a wrapped structure, it takes the form of 0D fullerenes, exemplified by C60 or buckyballs—a carbon molecule comprising 60 atoms arranged in a soccer ball-like structure. Alternatively, when graphene is rolled, it manifests as 1D nanotubes (CNT), characterized by a cylindrical wire-like structure with nanometer-scale dimensions, available in single-wall or multi-wall configurations. Finally, graphene, when stacked with more than 10 layers, is classified as 3D graphite (Nasir et al., 2018).

High functional group density, Larger specific area of surface, great chemical abilities and corrosion resistance are few of the distinctive physiochemical properties of

graphene oxide (GO) (Wang et al., 202;). GO surface has abundant oxygen and hydroxyl groups for adsorption, which also facilitate the addition of new functional groups and ligands for improving adsorption capacity (Tang et al., 2018). Unlike traditional nanomaterials that suffer from aggregation problems, the GO in this research will be modified with dendritic branches that will minimize the aggregation due to steric and electrostatic repulsion between the nanoparticles (Kim et al., 2022). Dispersion stability and strong anionic terminating groups will benefit the binding of cationic ions of metal from the aqueous solution (Kim & Park, 2017).

Through chemical or physical functionalization, graphene derivatives, especially GO, might be altered with a variety of organic or inorganic compounds. These materials can interact with other molecules in a covalent, non-covalent, or hybrid manner due to the accessibility of various groups that contain oxygen and the existence of sp^2 domains (Liu et al., 2022). As a result hybrid or composite materials are created that have a specific set of characteristics and possible uses, such as an improvement in dispersibility, processability, device manufacturing, biocompatibility, purification, and band gap alteration (Jimenez-Cervantes et al., 2016).

In this regard, current research focused on GO-based adsorbents with superior adsorption capacity to remove Pb from water. It was expected that GO composites would have high Pb adsorption in a wide pH range and would not be susceptible to the variations in Pb concentration in the contaminated water.

1.5. Background of Dendrimers

The inaugural dendrimer, poly(amidoamine) (PAMAM), was pioneered by Tomalia and collaborators. The synthesis involved cultivating it from a three-branched core, generated by the reaction of ammonia with methyl acrylate, succeeded by an excess of ethylenediamine. This two-step process can be iterated to produce subsequent generations, each featuring twice the number of branches as the preceding one. Notably, at the termination of each branch resides a free amino group, presenting promising applications in both biology and chemistry (Lyu et al., 2019).

Acetylated poly(amidoamine) (PAMAM) was synthesized through reactions between PAMAM and acetic anhydride. Following the acetylation of the outer layer, the dendrimer acquired water solubility, making it applicable for reducing the toxicity of 5-Fluorouracil (5FU) and facilitating drug delivery. Moreover, dendrimers prove

valuable as carriers in gene therapy. PAMAM, in particular, serves as a useful transfection reagent for delivering oligonucleotides containing antisense and plasmid expression vectors encoding antisense mRNA. Surprisingly, it has been found that picomolar concentrations of particular oligonucleotides, when administered via dendrimers, can exactly inhibit intended gene expression. This underscores the potential of dendrimers in precise and efficient therapeutic applications (Bacha et al., 2023; Jianli, 2011).

In addition to its applications in biology, PAMAM finds utility in various chemical processes. The abundance of functional groups and high solubility make dendrimers, in particular, valuable as nanoscale catalysts. For instance, PAMAM-encapsulated palladium (Pd) nanoparticles were synthesized and employed as catalysts for the Heck reaction. This novel catalyst demonstrated remarkable efficiency, yielding excellent results under phosphine-free conditions and utilizing 200 - 400 times less Pd than conventional catalysts, showcasing the potential of dendrimers in enhancing catalytic processes at the nanoscale (Woehler et al., 2003).

PAMAM has emerged as a versatile adsorbent owing to its numerous functional groups. When full-generation PAMAM dendrimers were coated inside the gaps of SBA-15 mesoporous substrates, Fadhel and colleagues observed a significant increase in CO₂ removal efficiency. This improvement was ascribed to the efficient outside dispersion of dendrimers within SBA-15, which made it easier for gaseous CO₂ to reach their amine groups. In a different application, When PAMAM was functionalized with chitosan was studied as an adsorbent for removing Hg (II), it was discovered that 5 was the ideal pH for the removal procedure. These findings underscore the adaptability of PAMAM in diverse adsorption scenarios, showcasing its potential in environmental and remediation applications (Geng et al., 2021).

1.6. Significance of the Research

Separation of nano sorbents from aqueous solution is problematic. Special equipment and high energy input for separation techniques hinder the application of nano sorbents on a large scale. In this study, GO was integrated with MNPs to impart a magnetic separation property in the composite. The magnetic field from the outside was used to separate the magnetic composite from the aqueous solution. This improved the outlook of sorbent from an economic perspective because it would not need expensive

equipment and/or energy-dependent separation techniques for recovering composite from the aqueous solution.

1.7. Research Objectives

The objectives of this research work were:

- Synthesize and characterize GO and MNPs
- Functionalize GO-MNP composite with dendritic structures and organic acids
- To investigate the role of terminal functional groups and GO weight percentage on lead removal
- Assessing the impact of pH, temperature, concentration, reusability, isotherm, and kinetic model on organic acid for Pb removal from aqueous solution

1.8. Aims of the Study

GO-based adsorbents with organic acid (vanillic acid (VA), gallic acid (GA), succinic acid (SA), and citric acid (CA)) functionalization were developed in this research to overcome the above-mentioned problems. The magnetic separation of the adsorbent from the aqueous solution guaranteed the full and effective recovery of GO from water. Functionalization decreased adsorbent aggregation by electrostatic repulsion and steric hindrance. This improved the number of operational adsorptive sites and the overall adsorption capacity of the composite. The research contributed towards the optimization of magnetic GO composites, yielding an apt interface between the magnetic nanoparticles (MNPs) and GO. The MNPs support magnetic separation and facilitate the removal of adsorbent from the aqueous solution.

LITERATURE REVIEW

2.1. Overview of Heavy Metal Contamination

Water is thought to be the most important resource for maintaining life and the environment in which we live. However, in today's age, a major crisis of water has been observed and it is reported that over eight billion humans are being affected by it, according to WWF. Pakistan is also facing a major water crisis where only 930 m³ of water per capita is accessible annually. Urban development, increasing industrialization along with increase in irrigation needs for the purpose of agriculture are known to be the major factors contributing to the depletion of quality and quantity of the country's water resources, resulting in reduced agricultural output, ultimately impacting the health of the population.

The existence of hazardous waterborne pollutants, particularly heavy metal ions such as Ag⁺, Hg²⁺, and Pb²⁺, in wastewater and natural water sources, represents a critical challenge to public health. Therefore, the development of efficient treatment technologies is imperative to mitigate these contaminants and reduce their concentrations to trace levels (ppb) (Wang et al., 2018). Pakistan's quality of water for drinking is rapidly declining as a result of the astonishing increase in the number of people and swift economic development of the nation. The WHO standards are not being met by the distribution of drinking water in urban areas (Daud et al., 2017).

In Pakistan, excessive lead in drinking water is ignored. In Karachi, an industrial city, high lead levels are a serious concern in many sources of drinking water. The WHO's acceptable limit of 10 µg/L is almost always exceeded in groundwater sources, which is especially concerning due to the high lead concentrations found in them. This emphasizes how urgent it is to address the possible health risks linked to elevated lead exposure in the affected areas by providing immediate attention and corrective measures. In half of Karachi's districts, the average lead content in ground water sources was greater than 150 µg/L (Ul-Haq et al., 2011). Lead concentrations in Zhob district, Quetta Valley, Baluchistan, Pakistan, ranged from 10 to 63 µg/L. A range of 1800 to 4700 µg/L of lead was detected in samples that were collected from Azad Jammu Kashmir's Pearl Valley (AJ&K) (Javaid et al., 2008). The majority of ground water samples in Hattar Industrial Estate (KPK) were found to be higher than the critical level

of 10 µg/L, with an average of 26 µg/L (Manzoor et al., 2006). In a comparable trend, 100% of the samples examined in Sialkot, the province of Punjab, had lead levels above the recommended threshold of 10 µg/L in drinking water (Rizwan et al., 2009). The observed lead concentration values pose severe health risks to the everyday users of contaminated water sources (Chandio et al., 2020).

2.2. Lead in Water

Lead has long been transported from its source into homes through the use of solder and plumbing materials that may come into contact with drinking water. Drinking water can have elevated lead concentrations due to leaching from lead contained in polyvinyl chloride (PVC) pipes. A few factors that influence the amount of lead dissolved are temperature, pH, water softness, standing time, and the existence of dissolved oxygen (DO) and chloride. Lead can leach from lead pipes quite easily, but research indicates that lead leakage from brass taps and soldered joints lessens over time (Tiwari et al., 2013).

Implementing corrosion control measures, including the accumulation of lime and adjusting the pH of the distribution system from less than 7 to 8 or 9, can effectively diminish the presence of lead in drinking water. Notably, lead exposure is still possible even after the water loses its plumbosolvent properties. This is explained by the fact of flaking lead carbonates that accumulate on lead pipes and iron build-up sediment. Lead can naturally contaminate ground and surface waters when storm water, which is often somewhat acidic, comes into contact with lead-contaminated soil. Lead can then dissolve in the water and find its way into nearby groundwater or surface waters. If enough lead is released into the environment, it may impact environmental receptors and have negative health effects on people if drinking water is obtained from these sources (Gaur et al., 2011).

2.3. Health Impacts of Lead

Heavy metals constitute a globally pervasive class of pollutants, primarily resulting from their widespread utilization in various industries. Famous for their wide distribution, these metals build up as hazardous waste in the human body's living tissues. Certain heavy metals are necessary as micronutrients for regular body processes, but excessive exposure to them can be harmful. The most toxic and

dangerous heavy metals are arsenic, lead, chromium, and mercury, according to the Office of the Health of the United States (Briffa et al., 2020).

There are several ways in which one can become exposed to heavy metals: ingestion through water or food, inhalation of dust or fumes, and physically touching them. Following absorption, these metals disperse throughout bodily tissues and organs. Metals are usually eliminated by the kidneys and digestive system, but they can also build up in certain storage locations like the liver, kidneys, and skeleton and remain there for years or even decades. Air and food sources can both expose people to lead in nearly equal amounts. Human exposure to lead has increased dramatically due to the utilization of lead in paint, ceramics, food cans, plumbing fixtures, and paint (Manual, n.d.).

Lead acetate was once used to sweeten port wine, and lead in food historically was derived from cooking and storage utensils. Significantly, the main source of lead emissions into the surrounding air was anti-knock agents, more especially lead organic compounds in fuel. Nonetheless, developed nations have seen a decrease in lead emissions, which has been linked to the widespread use of unleaded gasoline. As a result, the general public's blood lead levels have decreased. Inorganic lead exposure at work is common in battery plants, smelters, mines, and the welding of lead-painted metal. Airborne lead has the ability to settle in the soil and then concentrate in leafy greens like spinach and root vegetables like onions, making their way into the human food chain (Natasha et al., 2020).

The lungs absorb about half of the inorganic lead that is breathed in. Children may absorb up to 50% of lead from food due to the distinctive features of their gastrointestinal tracts, whereas adults normally absorb only 10% to 15% of it. Lead is mostly eliminated through urine and primarily binds to erythrocytes in the blood. In addition, lead has a half-life of roughly 20–30 years and accumulates in the skeleton. Adults have a well-developed blood-brain barrier that provides protection against external threats. Nonetheless, may suffer brain damage because their blood-brain barrier is still developing and there is a greater chance of lead entering the brain. Tetramethyl and tetraethyl lead, which are used in gasoline as anti-knock compounds, are easily absorbed through the skin and can cause lead encephalopathy (Järup, 2003). Restlessness and insomnia are among the symptoms of lead encephalopathy. Additional symptoms of acute lead poisoning include headache, moodiness, digestive discomfort, and other manifestations. Children who are exposed to lead for an extended period of

time at low levels may experience cognitive decline. Damage to the proximal renal tubules may result from acute lead exposure. Additionally, studies show that certain genetic and environmental variables may intensify the negative effects of lead on the development of the nervous system (Danielyan et al., 2019).

2.4. Applications of Graphene based materials

2.4.1. Graphene based materials for Filtration

Graphene's thinnest possible layer directly affects water permeability, which is its main advantage. Due to the separated pi orbitals on each side of its structure, pristine graphene acts as an impermeable barrier to water in its natural state, preventing the passage of any material. Nevertheless, by adding pores to the graphene sheets, this restriction can be removed. It is possible to deliberately design these pores so that they can hold onto other impurities while still allowing water molecules to flow through. These pores can be produced by a variety of techniques, such as subjecting the graphene coating to a gallium ion gun, which causes defects that, when exposed to an acidic solution, cause permeable pores to form (Ge et al., 2020).

By controlling graphene's time in contact with acid, the size of these openings can be managed precisely. Various methods of using graphene's properties for air and water filtration have been investigated by countless researchers. For the purpose of filtering substances such as Rose Bengal and methylene blue, Vishwanath et al. used a multilayer graphene/cellulose composite. The final composite showed remarkable filtration efficiency, with percentages for Rose Bengal reaching 94% and methylene blue reaching 98% (Vishwanath et al., 2022).

Gayen et al. used GO in filtering the water of the river. The results showed a notable disparity in outputs between the graphene filter and one without it. Using the GO filter, the iron removal efficiency increased from 70.7% to 84.5%. Hardness removal also demonstrated a significant improvement, increasing from 61.34% in the absence of a GO filter to 86.55% in the presence of one. Adding a GO filter increased the amount of arsenic removed from 82% to 90.9%. Applying the GO filter increased the removal efficiency of fluoride from 58% to 73.1%. These results highlight the usefulness of GO in enhancing the efficacy of different contaminants' removal from river water (Gayen et al., 2023).

The field of filtration shows great potential for graphene, which can be applied to reverse osmosis for the filtration of salted water. Graphene nanoplatelets crosslinked with polydopamine were used by Ndlwana et al. to study mixed matrix membranes. Significant improvements in rejecting salts like NaCl and MgSO₄ were observed by them, with graphene added reaching 99.85% and 99.95% of the total. Based on the combined findings, graphene appears to be a promising material for many filtration applications, indicating its effectiveness and adaptability in water treatment systems (Ndlwana et al., 2020).

2.4.2. Graphene based materials as Photocatalyst

As an improved oxidation process, photocatalytic degradation has become the preferred technique for treating wastewater. This approach is particularly effective in breaking down challenging organic chemicals, including dyes, which may resist decomposition through traditional methods. Graphene, with its porous structures featuring an increased number of trapping sites, proves adept at securely anchoring semiconductors. Because of this characteristic, graphene can efficiently take in electrons from these electronic devices, which shortens the time required for the electron-hole combination. Furthermore, the wavelength span absorbed by the photocatalyst is expanded by graphene's capacity to capture light, improving the photocatalytic process' overall efficacy (Levchuk et al., 2020).

Researchers have made significant strides in enhancing the performance of photocatalysts by developing graphene composites with various semiconductors. For example, mixing reduced graphene oxide with graphitic carbon nitride, showed enhanced photocatalytic removal of bisphenol A. This metal-free rGO/g-C₃N₄ photocatalyst exhibited enhanced efficiency in the breakdown of bisphenol A when exposed to visible light. A composite of cobalt ferrite and graphene nanoplatelets was effectively synthesized. They observed a significant rise in photocatalytic activity for the breakdown of methylene blue, which increased from 38.3% to an astounding 98.7%. Because graphene can prevent electron-hole pairs in semiconductors from recombining, this improvement has been attributed to it. Yan et al. produced a graphene/polypyrrole composite in a different study, and they used photocatalytic degradation to achieve an amazing 94.8% removal efficiency for phenol. These illustrations demonstrate the adaptability and efficiency of graphene-based composites in promoting the degradation

of different pollutants through photocatalysis (Chen et al., 2021; Israr et al., 2020; Yan et al., 2022).

2.4.3. Graphene based materials for Adsorption

Heavy metal adsorptive removal from water has been achieved through the development of ion exchange, biochar, activated carbon, MXenes, metal-organic frameworks (MOFs), and polymeric nanomaterials (Barkade et al., 2022; Rashida & Abdul, 2020). Such materials suffer from low functional densities, stability in aqueous solutions, inconsistent functional group distribution, problematic regeneration, and reusability (Shahzad et al., n.d.; Yosef et al., 2020). Nanomaterials have gained attention for adsorptive removal of Pb from water, Synthesis and optimization of nano-sorbents for Pb removal from water and wastewater is challenging.

GO was used previously for the adsorption of heavy metals from the liquid phase. Magnetic GO chitosan nanohybrid (MGC) was utilized for the elimination of Hg (II) from an aqueous solution (Bulin et al., 2023). The adsorption performance of GO for the removal of Pb (II) and Cd (II) from water was enhanced by the use of ionic liquids, such as potassium hexafluorophosphate (PF6) and 1-octyl-3-methylimidazolium hexafluorophosphate (CP8) (Al-Qahtani, 2017). Polyethyleneimine (PEI) was integrated with GO for the adsorptive removal of Cu (II) from water (Kuang et al., 2022). Magnetically separable GO (MGO) functionalized with lignin composite was also reported for Pb (II) and Ni (II) removal from aqueous solutions (Du et al., 2022). A Zinc oxide (ZnO) decorated on GO was used for the adsorption of Cr (VI) from aqueous solution (Singh et al., 2022).

2.5. Synthesis of Nanoparticles

A range of conventional techniques, such as chemical, photochemical, electrochemical, and biological ones, are used to create nanoparticles in various sizes and shapes. The requirements of different applications are taken into consideration when choosing the methods. The traditional techniques used to create nanoparticles are chemical and physical ones. Evaporation, condensation, and laser absorption are examples of physical methods, also known as instrumental approach. While the Solgel process, microwaves, hydrothermal method, chemical precipitation, and chemical vapor deposition are among the chemical synthesis approaches (Alvarado & Puga, n.d.).

2.6. Lead Removal Technologies

2.6.1. Electrodialysis

One popular electro-active method for treating wastewater is electrodialysis (ED), which is mainly used to desalinate water. This approach makes it easier to remove pollutants by applying a voltage electrode and allowing it to pass through an ion exchange membrane (IEM). Despite its effectiveness, the electricity consumption associated with ED limits its widespread application. Recent advancements in the electrochemical (EC) process have focused on improving efficiency, particularly through modifications to ion exchange membranes (IEMs).

A unique heterogeneous ion exchange membrane intended to exclude Pb^{2+} and other metal ions was presented by Nemati et al. This membrane separated Pb^{2+} ions from the solution with a 99.9% separation efficiency, demonstrating remarkable efficiency. This study shows that chemical modifications to IEMs are useful for improving system efficiency. Hosseini et al. went one step further and created a heterogeneous IEM for mixed-matrix electrodialysis using a functionalized composite of polyaniline (PANI) and graphene oxide (GO). The membrane's characteristics were enhanced by the addition of graphene oxide and polyaniline, which led to a 50% increase in Pb (II) flux over the pristine membrane. Promising outcomes have also been observed when combining the ED process with other methods. Pb removal using integrated adsorption and photo electrodialysis, with a 90% removal rate. This process, utilizing Algerian bentonite as an adsorbent, demonstrated the potential to reduce remaining Pb (II) levels to the threshold limit under artificial light and sunlight (Hosseini et al., 2018; Nemati et al., 2017).

2.6.2. Hydrogel

Hydrogels have been studied extensively for their ability to remove metallic ions, such as Pb (II), from sources of contaminated water due to their high-water content. They are also well-suited for capturing foreign ions from water. Chu and colleagues created a polyvinyl alcohol/polyacrylic acid double network gel (PVA/PAA gel) to extract lead (II) from water that had been contaminated. Even after the fifth cycle of use, this hydrogel sustained a constant removal efficiency of 100% and demonstrated an amazing capacity for adsorption of 194.99 mg/g for Pb (II).

To create a "nano-tentacle," a recent study used in situ growth of 3-aminopropyl trimethoxy silane on the innermost layer of a chitosan/graphene oxide combined porous gel (CGG). With an astounding uptake capacity of 470 mg/g, the resultant material, NT-CGG, showed ultrahigh affinity for Pb (II). The removal efficiency was higher than 99.9% even at lower concentrations (10 mg/L). By gelatinizing UiO-66-NH₂ and using ZrCl₄ to encourage cluster formation, Zhao et al. created amorphous Zr-MOG12, a metal-organic framework. This material had an extremely porous and amorphous structure and removed Pb (II) with exceptional efficiency. Hydrogels' superior Pb (II) and heavy metal removal performance from contaminated aqueous mediums has also been noted in other reports (Cheng et al., 2020; Zhao et al., 2020).

2.6.3. Photocatalytic process

The efficiency of TiO₂ and ZnO as photocatalysts in eliminating and converting various pollutants has been thoroughly investigated, making them popular choices. While the technique itself is considered sustainable and environmentally friendly during operation, concerns arise at the fabrication stages of the photocatalyst due to environmental implications.

Some researchers have taken a green approach during the fabrication stages in order to address these concerns; however, Pb (II) removal still presents difficulties. You et al.'s study used a simple hydrothermal technique to create a Bi₂O₃-TiO₂ composite. We next investigated the possibility of removing Pb (II) and degrading dibutyl phthalate (DBP) simultaneously using photocatalysis on this composite. Notably, the study showed that photoinduced holes and electrons traveled independently to various sites, increasing the number of photocatalytic reaction sites that could be used for DBP degradation and Pb (II) reduction (You et al., 2018; Zinatloo-ajabshir et al., 2020).

2.6.4. Membrane filtration

Membrane filtration is a commonly used method for eliminating a wide range of contaminants from drinking water and wastewater, such as pesticides, heavy metals, organic compounds, and microbes. The degree of hydrophilicity, the size and distribution of pores, surface charge, solution flow, and the presence of functional groups that facilitate pollutant separation all play a role in the selection of the best membrane for treating contaminated wastewater. These characteristics of the membrane have a major effect on the rate of water production and separation efficiency. Adsorptive

membranes, UF, NF, RO, and FO are among the membrane technologies that have been thoroughly studied in the particular context of Pb (II) removal (Hube et al., 2020; Pronk et al., 2019).

2.6.5. Electrodeposition

In addition to plating and decorating items for a variety of uses, electrodeposition is a flexible technique that is frequently used to remove and recover metals from water and wastewater. The metal depositing material, as well as additional factors like dendrite formation, side reactions (like H₂ evolution), and process stability, all have an impact on how efficient the electrodeposition process is. Pb (II) was nearly entirely removed by electrodeposition on a hydrotalcite electrode in a study that used two hydrotalcite-like compounds as substrates. Two mechanisms, adsorption, and electrodeposition, worked in tandem to remove the material.

Zhang and colleagues have presented a novel approach to remove lead (II) from smelting wastewater: bioelectrochemically-assisted electrodeposition, or BES-EDP. Using graphite and carbon brushes as the anode and cathode, respectively, and an external circuit to link them, this system had two chambers divided by an anionic exchange membrane. The results showed a 98% removal of Pb (II) in 10 hours. Additionally, the study observed that during Pb (II) reduction, metal oxides are formed and have an effect on the electrodeposition process (Kumar & Dwivedi, 2021; Zhang et al., 2020)

2.6.6. Adsorption

The solid surface's attraction to the gas or liquid particle particles causes this phenomenon. The nature of the adsorbate, the adsorbent material's properties, temperature, pressure, and the amount of surface area available for adsorption are some of the factors that contribute to adsorption's effectiveness. A number of adsorbents have been investigated with encouraging results. Adsorbent cost, surface chemistry, porosity, and surface area are some of the variables that can affect how effective it is. It is noteworthy that a number of factors, including temperature, the dosage of the adsorbent, the occurrence of other competing ions in the solution, and the initial concentration of Pb (II), can affect how well Pb (II) is removed through adsorption. Consequently, in order to remove chromium from water sources in an effective and affordable manner, maximizing the efficiency of these parameters is crucial (Qasem et al., 2021).

Many contaminants, including dyes, pesticides, organic pollutants, nutrients like phosphorus and nitrogen, and heavy metals like Pb (II), have been extensively studied and removed using the adsorption method. This approach has attracted widespread scientific interest. The efficacy of various readily available and reasonably priced adsorbent materials in treating industrial wastewater has been investigated over the years. Clay soil, zeolite, municipal waste, sludge waste, and biomass from agricultural waste are a few examples. In addition, the adsorption capabilities of processed and functionalized materials like activated carbon, activated zeolite, hydrochar, biochar, and nanomaterials have been thoroughly researched. These materials provide effective and adaptable ways to treat industrial wastewater (Boeykens et al., 2019; Thabede et al., 2020).

MATERIALS AND METHOD

3.1. Chemicals

Graphite powder, Sulphuric acid (H_2SO_4), Boric acid (H_3BO_3), Potassium permanganate (KMnO_4), Hydrochloric acid (HCl), Iron (II) chloride hexahydrate ($\text{FeCl}_3 \cdot 6\text{H}_2\text{O}$), Iron (II) sulphate heptahydrate ($\text{FeSO}_4 \cdot 7\text{H}_2\text{O}$), Hydrogen peroxide (H_2O_2), Ammonium hydroxide (NH_4OH), 3-amino propyl trimethoxy silane ($\text{C}_9\text{H}_{23}\text{NO}_3\text{Si}$, APT), Methyl acrylate ($\text{C}_4\text{H}_6\text{O}_2$), 1-ethyl-3-(3-dimethylaminopropyl) carbodiimide hydrochloride ($\text{C}_8\text{H}_{17}\text{N}_3 \cdot \text{HCl}$, EDC), N hydro succinimide ($\text{C}_4\text{H}_5\text{NO}_3$, NHS), Citric acid ($\text{C}_6\text{H}_8\text{O}_7$), Gallic acid ($\text{C}_5\text{H}_9\text{ON}_4$), Succinic acid ($\text{C}_4\text{H}_6\text{O}_4$), Vanillic acid ($\text{C}_8\text{H}_8\text{O}_4$), Lead standard solution (1000mg/L), Ethylenediamine anhydrous ($\text{C}_2\text{H}_8\text{N}_2$) and Methanol.

3.2. Characterization Instruments

A transmission electron microscope (TEM, JEM 2100F, JEOL, Japan) was utilized to investigate the morphological characteristics of the nanoparticles. The sample was made by ultrasonically dispersing nanocomposites in methanol for five minutes. On a 300-mesh copper TEM grid, a drop of dispersed nanoparticles was dropped for analysis. The crystalline structure of composites was examined using an X-ray diffractometer (XRD, DRON 8, BRUKER UNITED STATES). The Horiba Scientific Raman diffractometer Xplora ONE, which has an exciting laser source of 532 nm, was used to measure the Raman shifts. Customized with energy dispersive X-ray spectroscopy (EDX; JED 2300, Jeol Ltd, Japan), the field emission scanning electron microscope (Fe-SEM-6330F, Jeol Ltd, Tokyo, Japan) was employed to assess the properties of the composites, including size, morphology, and purity. To look into how synthetic nanoparticles are chemically bonded, a Fourier Transmissilicon Infrared (FT-IR) spectrometer (TENSOR27) was purchased. Thermogravimetric analysis (TGA, SDT Q600, Auto-DSCQ20, TA Instruments, USA) was utilized to measure the organic weight loss. To test the surface zeta potential of nanoparticles, Zetasizer (Nano ZS90, Malvern, UK) was employed. ICP-OES (inductively coupled plasma optical emission spectrometry) (Optima ICP-OES 8000, Perkin Elmer) was implemented to examine the concentrations of metal ions in the supernatant.

3.3. Methodology Overview

The schematic diagram presented in figure 1 illustrates the methodology employed in this study. The process commenced with the individual synthesis of Graphene Oxide (GO) and Magnetic Nanoparticles (MNPs). Subsequently, Magnetic Graphene Oxide (MGO) was synthesized, with variations in weight percentages from 20 to 70. Among these, GMNP 40 was selected for further functionalization with dendrimers. In the subsequent phase, GMNP 40 underwent dendrimer functionalization. This critical step involved the fabrication of dendrimer-functionalized Magnetic Graphene Oxide Nanoparticles (GMNPs) using four different acids: Citric Acid (CA), Vanillic Acid (VA), Succinic Acid (SA), and Gallic Acid (GA).

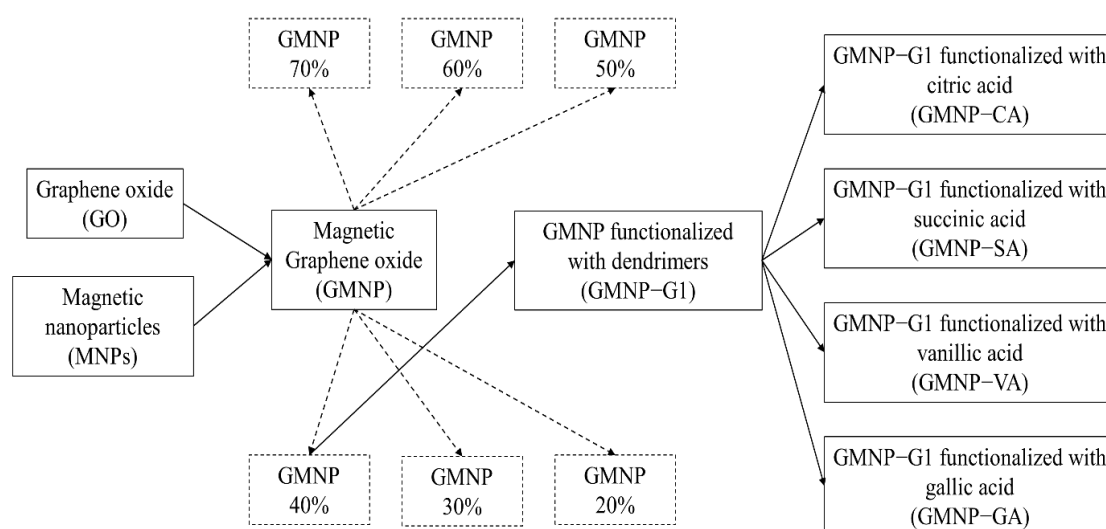


Figure 1: Schematic diagram of the methodology

3.4. Synthesis of Graphene oxide

GO was prepared using hummer's method (Yosef et al., 2020). Precisley, 50mL of H_2SO_4 and 0.5g of H_3BO_3 were taken in a glass beaker. The beaker was placed in an ice bath and 1.5g of Graphite powder was added under stirring. Slowly, 6g of $KMnO_4$ were added while keeping the temperature below $15^\circ C$ and stirred for 15 mins. It was heated to $35^\circ C$ for 18h or until the solution becomes like foam. By slowly adding 50mL water, the temperature was raised due to hydration heat and kept at $90^\circ C$ for 30 mins. Subsequently, it was cooled to room temperature. After addition of 150mL water, 1mL H_2O_2 was added slowly to obtain a yellowish mixture. The mixture was separated by

centrifugation at 6000 rpm (20 mins). The washing was done two times with HCl (5%) and three times with water to remove metal ions. For each time washing sonicate for 15 mins and centrifuge at 6000 rpm for 20 mins. Dried in oven at 60°C for 24h. The powder was crushed and transferred to vacuum filtration. It was filtered until pH became between 6 and 7. Finally, it was dried in an oven at 60°C for 24h.

3.5. Synthesis of Magnetic Nano particles

Magnetic nanoparticles (MNPs) were synthesized by using salts of iron, FeSO₄, and FeCl₃. Briefly, 5.7g of FeCl₃.6H₂O and 2.7g of FeSO₄.7H₂O were added to 100 mL of DI water and placed in an ultrasonic bath for water and 30 mins for further dispersion (Kim et al., 2019). The mixture was transferred to a rotary evaporator. The temperature was raised to 80°C for 30 mins at 120 rpm. NH₄OH aqueous solution was added drop wise to precipitate the iron oxides. The obtained precipitate was collected by a suitable magnet, washed with 100 mL of DI water five times, and dried at 60°C overnight in the oven.

3.6. Synthesis of Graphene oxide magnetic nano particles

Graphene oxide magnetic nanoparticles (GMNP) were synthesized by the chemical co-precipitation of FeSO₄ and FeCl₃ in the presence of GO (Du et al., 2022; Kuang et al., 2022). Briefly, 0.5g of GO, 0.95g of FeCl₃.6H₂O, and 0.45g of FeSO₄.7H₂O were added to 100 mL of DI water and placed in an ultra-sonic bath for 30 mins for further dispersion. The mixture was then transferred to a rotary evaporator. The temperature was raised to 50°C for 10 mins at 120 rpm. NH₄OH aqueous solution was added drop wise to precipitate the iron oxides. Then, in order to modify the adsorbent, the mixture was stirred for 30 mins at 80°C and 120 rpm. The obtained precipitate was collected by a suitable magnet, washed with 100 mL of DI water five times, and dried at 60°C overnight in the oven. The nano composites with different Fe₃O₄:GO weight percentages of 50, 40, 30, and 20 were synthesized.

3.7. Synthesis of Graphene oxide magnetic nanoparticles

Dendrimers

Precisely, 200 mL of methanol were added to 2g of GMNP (Kim & Park, 2017). The GMNP suspension was gradually stirred with 10 mL of APT for seven hours at 60°C. The GMNP that was altered using APT in this study was referred to as "generation 0"

of GMNP-G0. After obtaining G0, it was five times cleaned with methanol and then re-dispersed in a solution that contained 20 mL of $C_6H_4O_2$ and 100 mL of methanol. The product was repeatedly washed with methanol after the solution had been vigorously stirred for seven hours at room temperature. The first generation of GMNP (GMNP-G1) was produced by dispersing the obtained products in a solution of methanol (20 mL) and ethylenediamine (4 mL) and stirring at room temperature for three hours. To get rid of any remaining reactants, the synthesized GMNP-G1 was cleaned five times with methanol and then dried for an entire night at 60°C in an oven. From now on in this manuscript, GMNP-G1 has been referred to as GMNP.

3.8. Functionalization of citric, gallic, succinic, and vanillic acid on GMNP

A carboxyl group and an amine underwent amide condensation to create functionalized organic acid GMNP (Kim et al., 2022). Carboxyl groups from organic acids were used to modify the amine groups in GMNP. In 30 ml of DI water, the EDC (0.288g) and NHS (0.173g) were dissolved. For 4 h at room temperature, the EDC-NHS solution was combined with 0.144g of CA and agitated vigorously. The prepared CA-EDC-NHS solution was added with 2g of GMNP that was initially ultrasonically dispersed in 50 mL methanol for 30 minutes. The CA-modified GMNP (GMNP-CA) was oven-dried for an entire night at 60°C after being five times cleaned with methanol. At room temperature and with stirring, the amide condensation reaction was finished in 18 h. In a similar synthesis protocol, the addition of CA to EDC-NHS was substituted with additions of GA (0.127g), SA (0.089g), and VA (0.126g) to produce the GA modified GMNP (GMNP-GA), SA modified GMNP (GMNP-SA), and VA modified GMNP (GMNP-VA). This outcome is shown in figure 2.

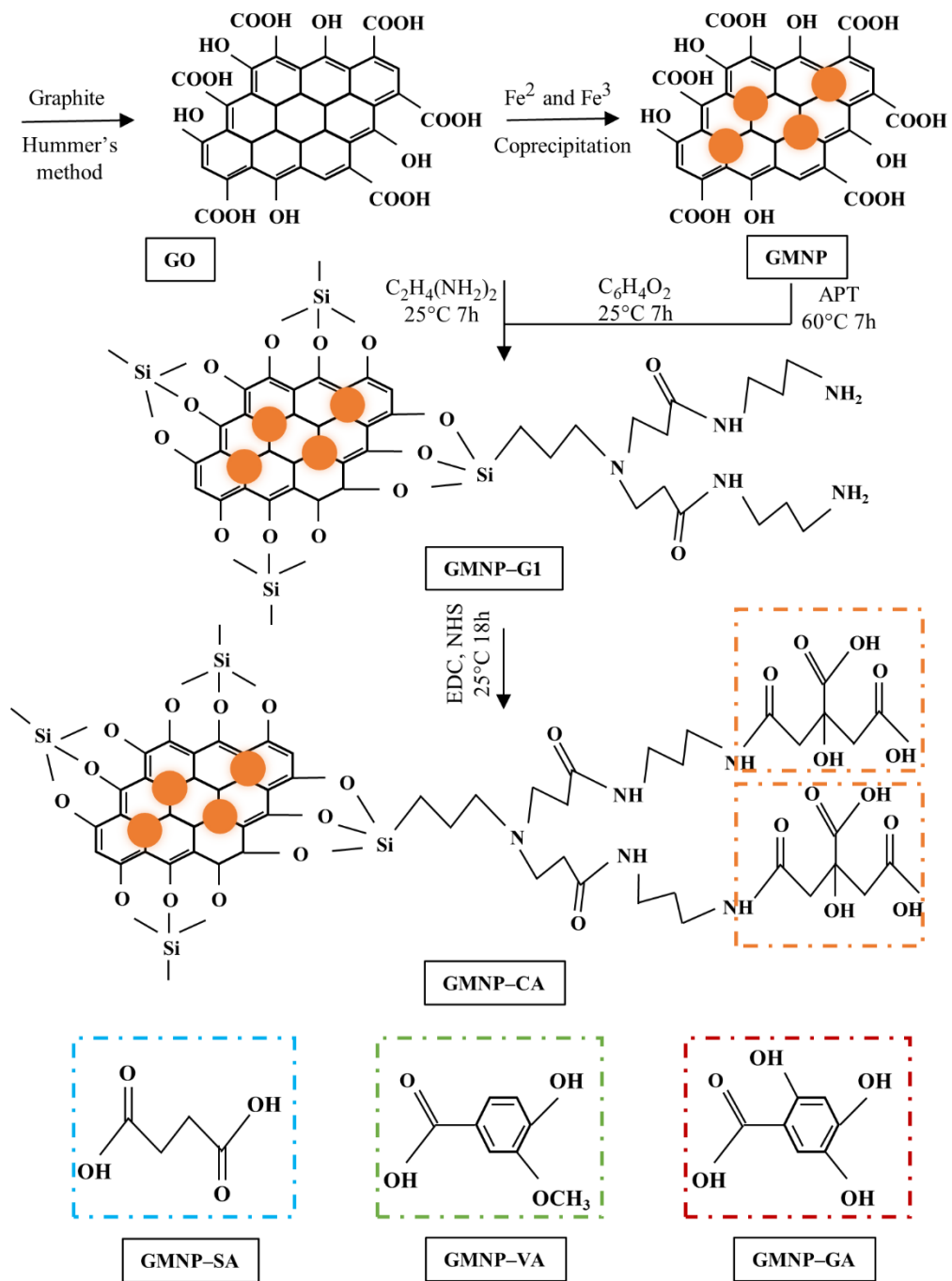


Figure 2: Schematic diagram of CA, SA, VA and GA functionalized GMNP synthetic procedure

RESULTS AND DISCUSSION

4.1. Characterization

4.1.1. TEM Analysis

Composites were subjected to Transmission electron microscope (TEM) characterization in order to see the splicing of the particles, as displayed in figure 3. Multiple GO sheets, along with their edges and corners, can be discerned in the TEM image of all composites. These edges can be seen throughout the composites, indicating the GO contours. Moreover, consolidated sphere-like particles with a diameter of about 30 nm were anchored to the GO surface in a regular pattern, that were mainly Fe₃O₄ (Yang et al., 2019). The amalgamated magnetic particles on the GO are clearly capable of acting as nanoscale barriers to prevent the replenishing of the GO, ensuring excellent adsorption properties. Accumulation, oxidation, and deterioration by an acidic environment were also adequately eluded and maintained the magnetic characteristics because the Fe₃O₄ particles were effectively wrapped inside the GO. The figure illustrated the distribution of Fe₃O₄ particles on the GO surface and the influence of Fe₃O₄:GO mass ratio (Xiao, 2015). The TEM image of GMNP-G1 reflects those dendrimers that makes up the majority of connected particles forming a chain-like configuration. The microscopic chain is originating from the dendrimer's carbon chain. Besides, as few particles were coated by GO. The layer interval is widened and p-p stacking of GO is prevented by surface-attached dendritic branches. The morphology of GMNP-CA, GMNP-VA, and GMNP-SA were also investigated by using TEM. The shape and size of particles were unaffected by step-by-step modification of GMNP-G1. After modification, organic acid functionalized GMNP-G1 (GMNP-CA, GMNP-VA, and GMNP-SA) still exhibited their original morphological traits. The composites have different levels of particle aggregation, and there was no discernible pattern to explain the extent of aggregation.

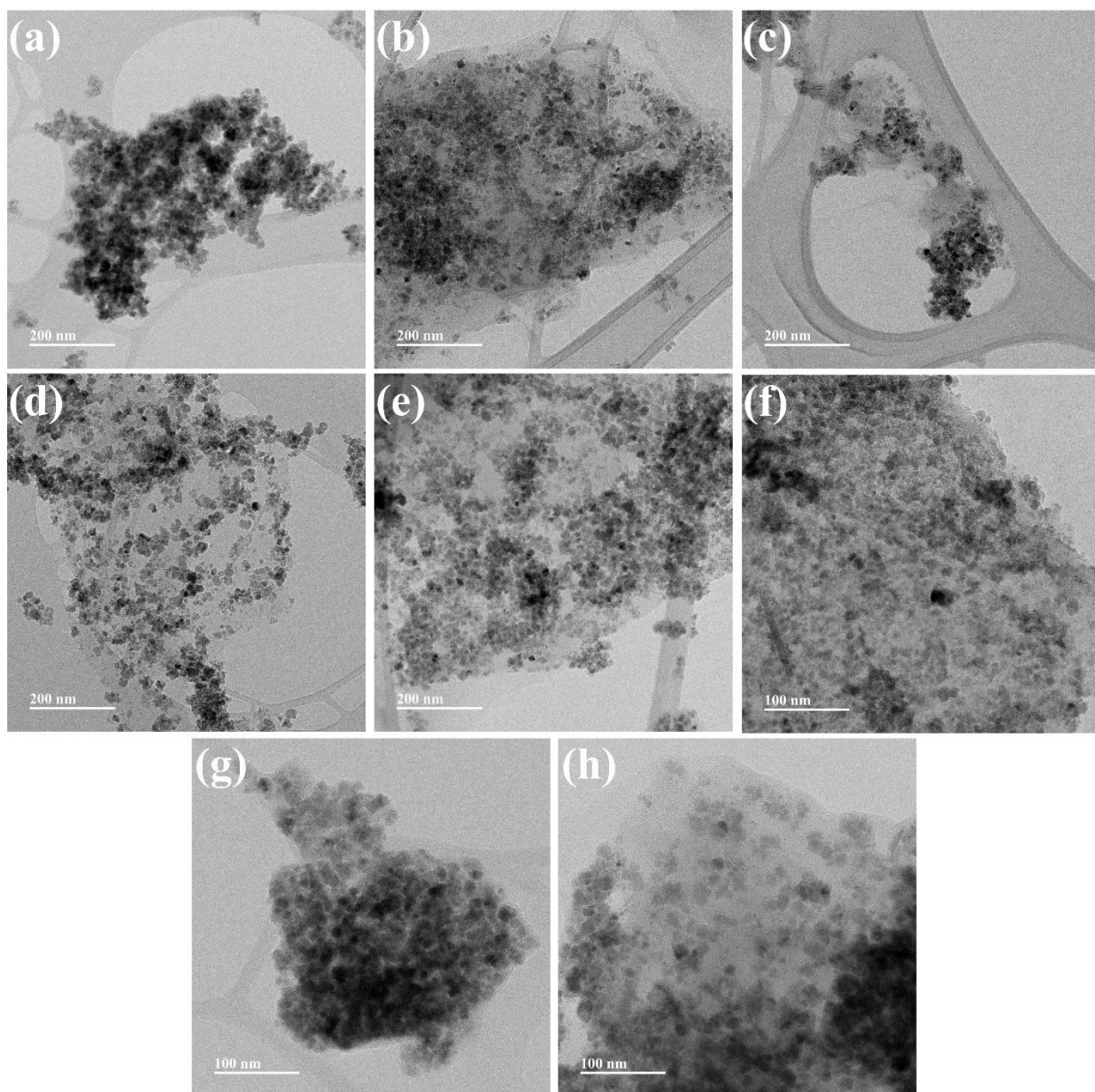


Figure 3: TEM images of (a) GMNP-50, (b) GMNP-40, (c) GMNP-30, (d) GMNP-20, (e) GMNP-G1, (f) GMNP-VA, (g) GMNP-CA, and (h) GMNP-SA

4.1.2. SEM Analysis

The topological morphology of MNP, GMNP-40, and GMNP-CA was analyzed by deploying a Scanning electron microscope (SEM), and the outcomes are presented in Figure 4. The MNP and GMNP-40 displayed a favorable texture, which allowed the nanoparticles to achieve a significant adsorption potential for heavy metal ions due to a greater specific region of the surface. The surface morphology of GO with a smooth layer was perceived in GMNP-40. However, GMNP-40 had patterns that were refined

and bigger than those of MNP, signaling that MNPs were well bound to GO (Neolaka et al., 2020).

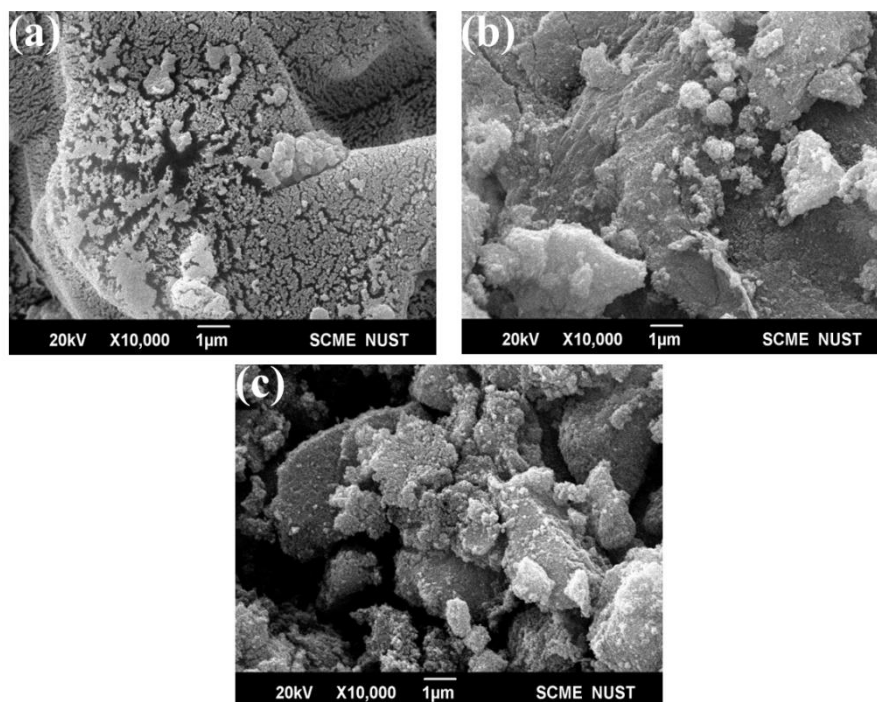


Figure 4: SEM images of (a) MNP, (b) GMNP-40, and (c) GMNP-CA

4.1.3. EDX Analysis

Additionally, the nanocomposite's composition was detected by EDX which can be observed in Table 1. The outcomes stated that the incorporation of Fe and N elements into GMNP had been successful and uniform. Meanwhile, O elements are evenly distributed, which could be beneficial for the absorption of ions from heavy metals. The Si K element could be noticed, as a result of the APTES that was grown to the GMNP surface after the dendrimer structure formed.

Table 1: EDX of MNP, GMNP-40, and GMNP-CA.

MNP		GMNP-40		GMNP-CA	
Element	Weight %	Element	Weight %	Element	Weight %
C K	59.23	C K	22.75	C K	19.4
O K	25.43	N K	15.15	O K	32.4
Fe K	15.33	O K	33.55	Si K	1.5
		Fe K	28.55	Fe K	46.7

4.1.4. XRD Analysis

XRD analysis was leveraged to typify the phase purity and crystalline nature of the synthesized GO. X-Ray diffractograms of Graphite, GO, MNP, GMNP, GMNP-G1, and GMNP-VA are represented in figure 5. The sharp diffraction peak of graphite at $2\theta = 26.5^\circ$, stipulates a distance between interlayers of 0.337 nm, which correlates with evocative spacing of the graphite plane allocated to (002). The distinctive graphite peak vanishes after oxidation and was replaced by a sharp peak at $2\theta = 11.5^\circ$, which correlates to the distance between interlayers of 0.771 nm and embodies the contrast of layer-like structure allocated to (001). After the graphite is transformed into GO, the distance between the interlayer increases from 0.337 to 0.771 nm. It is explained by the profusion of functional groups containing oxygen on the GO surfaces (Serol & Gökhan, 2018). At the same time, the XRD pattern of GO exhibits a wide peak at $2\theta = 24.1^\circ$ with 0.369 nm d spacing, which is significantly comparable with the GO, proving the restoration of the reduced ordered graphitic crystal structure. The peaks at $2\theta = 32.6^\circ$, 35.7° , 40.3° , 52.9° , 58.3° , and 68.4° correlate with the cubic overturn spinel crystalline structure of Fe_3O_4 . The reflections of (220), (311), (400), (422), (511), and (440) can be attributed to these peaks, respectively (Thy et al., 2022). The reduction of the GO peak also reveals that Fe_3O_4 nanoparticles were attached to the GO surface, resulting in the larger interlayer spacing between the GO structure. There were the same GMNP-related diffraction peaks in the GMNP-G1 and GMNP-VA, showing that functionalization had very little impact on the integrity of GMNP. There was a slight decrease in GMNP-G1 peaks. The results of XRD analysis verified that the technique of modification could produce composites with good stability.

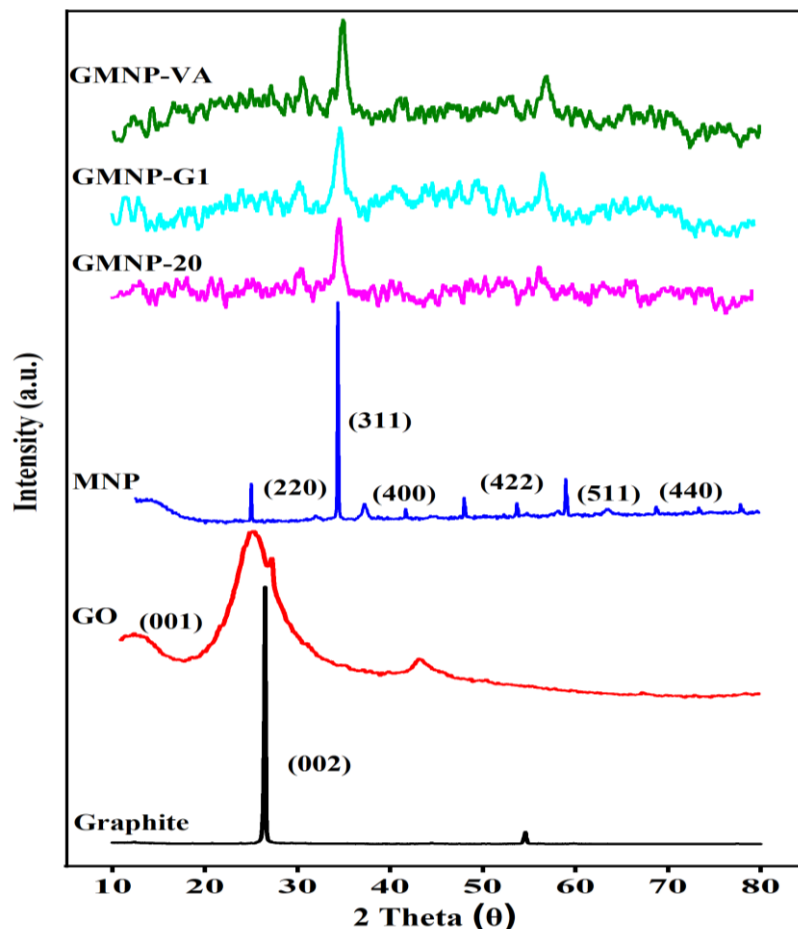


Figure 5: XRD Graphite, GO, MNP, GMNP-20, GMNP-G1, and GMNP-VA.

4.1.5. RAMAN Analysis

Raman spectroscopy is a common nondestructive testing to understand the structural makeup of carbon-based materials. Raman spectra of Graphite, GO, GMNP, GMNP-G1, and GMNP-VA are represented in Figure 6. Raman spectrum of Graphite and GO interprets the three distinctive peaks of graphite materials i.e., D, G, and 2D modes at 1348, 1592, and 2723 cm^{-1} respectively (Albert et al., 2018). The vibration caused by stretching of the sp^2 C=C bonds in the graphitic hexagonal structure is what causes the G mode peak to manifest. On the other hand, oxidation-related D mode peaks show the existence of sp^3 carbon centers. The existence of a few layered graphene is demonstrated by the 2D mode peak, which reflects at a lower frequency when compared to parent bulk graphite. A peak at 600 cm^{-1} can be seen in the GMNP spectrum which is due stretching of the Fe–O bond, similar peaks can be noticed in the GMNP-G1 and GMNP-VA spectra with a small decrease in the peaks. Further, measuring the ID/IG ratio enables to figure out the defects of materials based on

graphene. The ID/IG ratio values for graphite, GO and GMNP are 0.04, 0.85, and 1.09, respectively. The ID/IG value of GMNP, GMNP-G1, and GMNP-VA increases from 0.85 to 1.09 after functionalization, corroborating the feasible functionalization. Fe₃O₄ particles act as steric barriers to the restacking GO through p-p interaction.

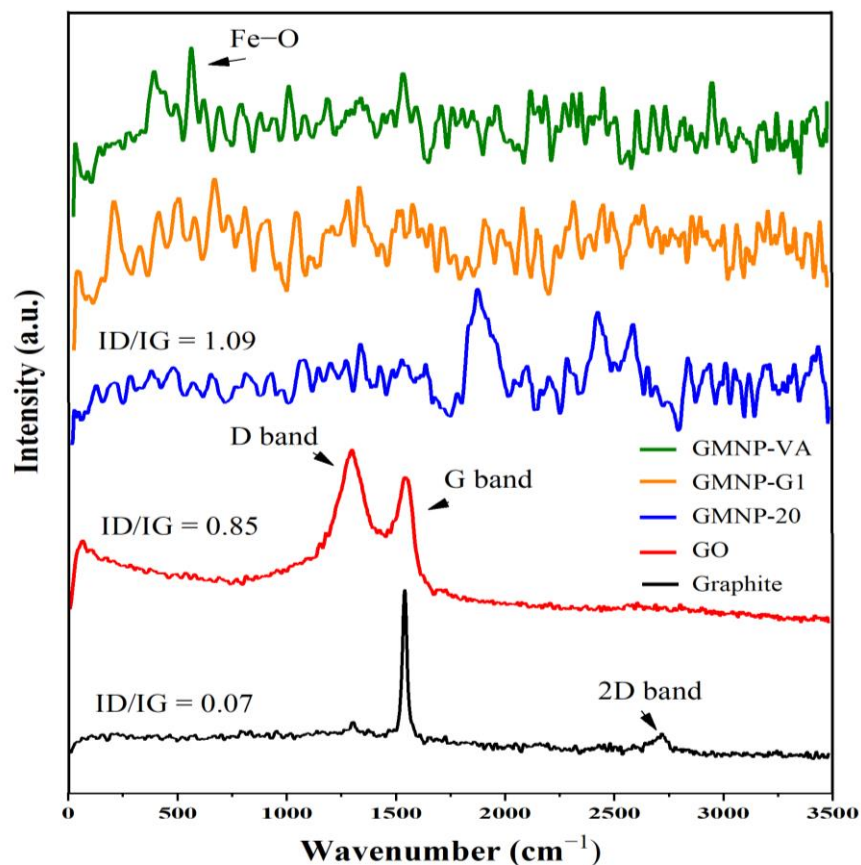


Figure 6: Raman spectra of Graphite, GO, GMNP-20, GMNP-G1, and GMNP-VA.

4.1.6. Functional groups identification

The functional groups were identified by performing the Fourier transmission infrared (FTIR) spectroscopy. Figure 7 articulates the characteristic features of composites. FTIR spectra of GO illustrates the attributed adsorption bands to the stretching of -OH, C=O, C-C, and C-O at respective peaks of 3427, 1709, 1604, and 1099 cm⁻¹ (Wang et al., 2022). The Fe-O stretching vibration is consigned to the strong signal at 564 cm⁻¹ and potent OH band at 3470 in the FTIR spectrum of MNPs. The OH band can be chalked up due to the remaining water that was not completely removed from the surface of the Fe₃O₄ particles. Akin peaks of Fe-O and GO were seen in FTIR spectra

of distinct percentage composites of GMNPs, affirming the encapsulation of various composites. Silane coupling agent bond (Si–O–Si) was discernible at 992 cm^{-1} , corroborating the moderation of APTES (G1) on GMNP. The stemming of carboxyl groups in CA, SA, VA, and GA reveals the stretching at 1450 cm^{-1} in organic acid functionalized GMNP-G1 (Peiman et al., 2021). The creation of a CO–NH bond between amine groups in GMNP-G1 and carboxyl groups in organic acids revealed from a prominent peak around 1570 cm^{-1} . The peaks around 2900 cm^{-1} are attributed to the symmetric or asymmetric stretch of the C–H bond in methylene groups. The bands at 3400 cm^{-1} correspond to N–H stretching and O–H bond of chemisorption. From FTIR results, we confirmed that functionalization was achieved on GMNPs with dendrimers and organic acids.

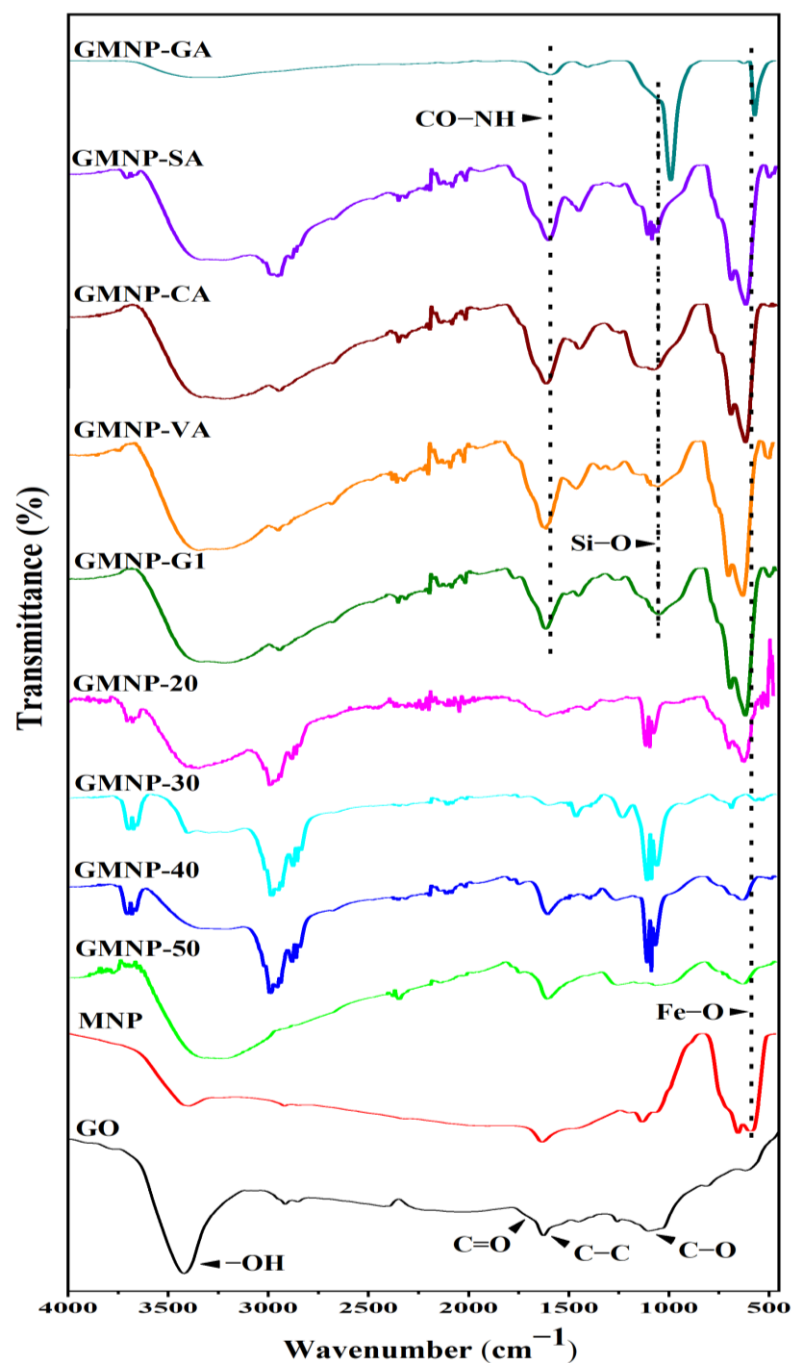


Figure 7: FTIR spectra of Graphite, GO, MNP, GMNP-50, GMNP-40, GMNP-30, GMNP-20, GMNP-G1, GMNP-VA, GMNP-CA, GMNP-SA, and GMNP-GA

4.1.7. TGA Analysis

Thermogravimetric analyzer (TGA) perusal evinces the multiple-stage weight loss in the nitrogen gas atmosphere as displayed in Figure 8. In the 40-200 °C temperature range, 2% weight that perished was due to the solvents and structure of water molecules that barely perturbed upon adsorption (Torabi Fard et al., 2022). An 8-9%

weight loss between 200-450 °C was elicited by Dendritic structure and Carboxyl moieties of organic acids on GMNPs. Juxtapose to GMNPs and GMNP-G1 weight loss with organic acid effectuate GMNP-G1 was unsubstantial, acquiesce the functionalization of organic acids on their surface. All the composites lose their respective weight above 450°C as the manifestation of depolymerization and pyrolysis of their structures. The final weight of GMNP-CA, GMNP-VA, and GMNP-SA were 89.8%, 86.3%, and 89.3%, respectively.

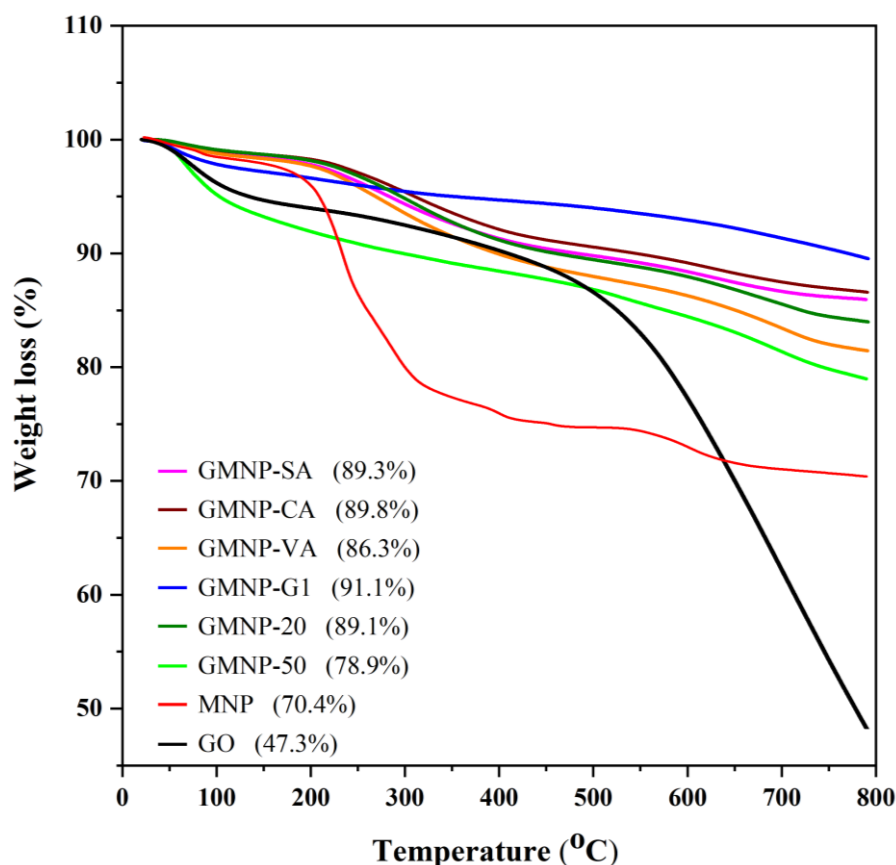


Figure 8: TGA analysis of GO, MNP, GMNP-50, GMNP-20, GMNP-G1, GMNP-VA, GMNP-CA, and GMNP-SA.

4.2. Performance Evaluation

4.2.1. Adsorption Studies

Pb (II) adsorption tests were carried out in batch mode at room temperature. For this, DI water was used to dilute the Pb (II) stock solution (1000 mg/L), and 1M NaOH and 1M HCl were used to adjust the pH for each experiment. The experimental solution volume and adsorbent concentration were adjusted to 50 ml and 100 mg/L, respectively. The mixture was agitated at 200 rpm for 24 hours while being sonicated for 1 min. The

influence of various factors on the adsorption process, including pH, initial solution concentration, temperature, and reusability was evaluated. Additionally, different kinetics and isotherms models were applied to examine the Pb (II) adsorption behavior of synthesized composites. The adsorbent was separated using a magnet from the solution. The polyvinylidene fluoride syringe filters (0.22 μ m) were used to filter the solution and Pb (II) experiment concentration was measured using ICP-OES. Equations (1) and (2) were used to compute and estimate the adsorption capacity (Q_t) and percentage of removal, respectively.

$$Q_t = \frac{(C_o - C_e) \times V}{W} \quad (1)$$

$$\% \text{ of Removal} = \frac{(C_o - C_e) \times 100}{C_o} \quad (2)$$

Where C_o (mg/L) and C_e (mg/L) are the initial and final concentration of Pb (II) solution, while the volume of the solution is V (L) and the weight of the adsorbent is W (g).

4.2.2. Performance Comparison

Figure 9 displays the various nanocomposites that were created and put through adsorption tests with initial Pb (II) concentrations of 50 mg/L, pH = 5, adsorbent dosage of 100 mg/L, contact time of 24 hours, and temperature of 303 K. Initially GO and MNP were developed, removing Pb (II) by 98% and 21%, respectively. Following that, 70 to 20 weight percentages of GO and MNP were formed (GMNP-70, GMNP-60, GMNP-50, GMNP-40, GMNP-30, and GMNP-20) showing the adsorption efficiency of 54, 56, 55, 51, 37 and 29, respectively. GMNP-70, GMNP-60, GMNP-50, and GMNP-40 illustrate similar results to one another. Then GMNP-40 was opted in order to functionalize with dendrimers (GMNP-G1). Pb (II) was removed by GMNP-G1 to the extent of 26%. Moreover, GMNP-G1 endured distinctive modifications with CA (GMNP-CA), GA (GMNP-GA), SA (GMNP-SA), and VA (GMNP-VA). The best outcomes are demonstrated by GMNP-CA, which removes Pb (II) by 94% whereas GMNP-SA, GMNP-GA, and GMNP-VA remove Pb (II) by 88%, 71%, and 66% respectively.

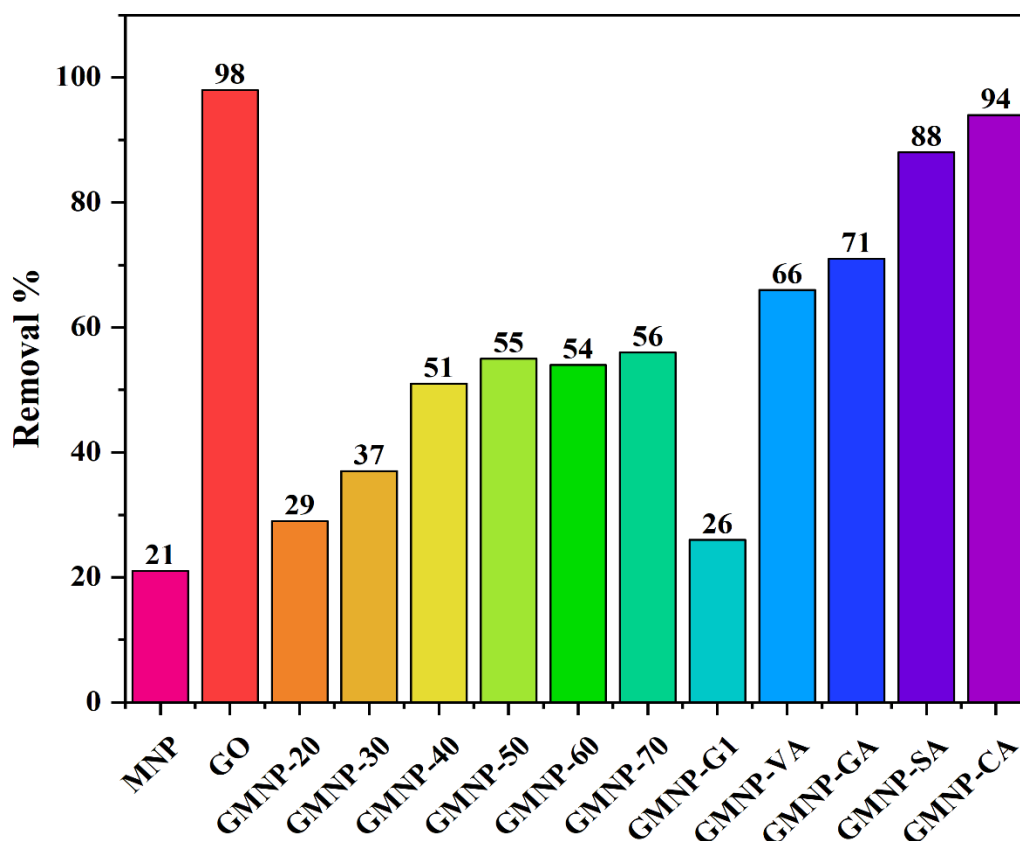


Figure 9: Removal Comparison of different composites (GO, MNP, GMNP-20, GMNP-30, GMNP-40, GMNP-50, GMNP-60, GMNP-70, GMNP-G1, GMNP-VA, GMNP-CA, GMNP-SA, and GMNP-GA)

4.2.3. Zeta Potential

The point of zero charge (pH_{pzc}) has direct relation with the synthesized nanocomposites as depicted in Figure 10. The pH at which the surface charge of nanocomposites is zero, is known as pH_{pzc} . The GMNP-40 showed a neutral surface charge at $\text{pH} = 6.2$, which changed to negative with a slight increase in $\text{pH} = 6.4$. The pH_{pzc} of GMNP-G1 was attained at the value of $\text{pH} = 9.5$. The determined values of pH_{pzc} of GMNP-VA, GMNP-GA, GMNP-CA, and GMNP-SA were determined at $\text{pH} = 8.3, 7.8, 4.3,$ and 5.5 respectively. The negatively charged surface on all composites was generally triggered by the ionization of hydroxyl and carboxyl functional groups at more acidic pH levels (Ahmad et al., 2020). Aqueous dispersion is more stable when these surface charges are produced as a result of mutual repulsion. Thus, from pH 8 to 10, the GMNP-G1, GMNP-VA, and GMNP-GA stayed positively charged, but at low pH, the GMNP-40, GMNP-CA, and GMNP-SA acquired a negative charge. Aggregation has the primary ability to decrease surface area and modify adsorption

properties during the dispersion phase. High surface area is ascertained by electrostatic repulsion to prevent the aggregation between the nanocomposites in the dispersion phase.

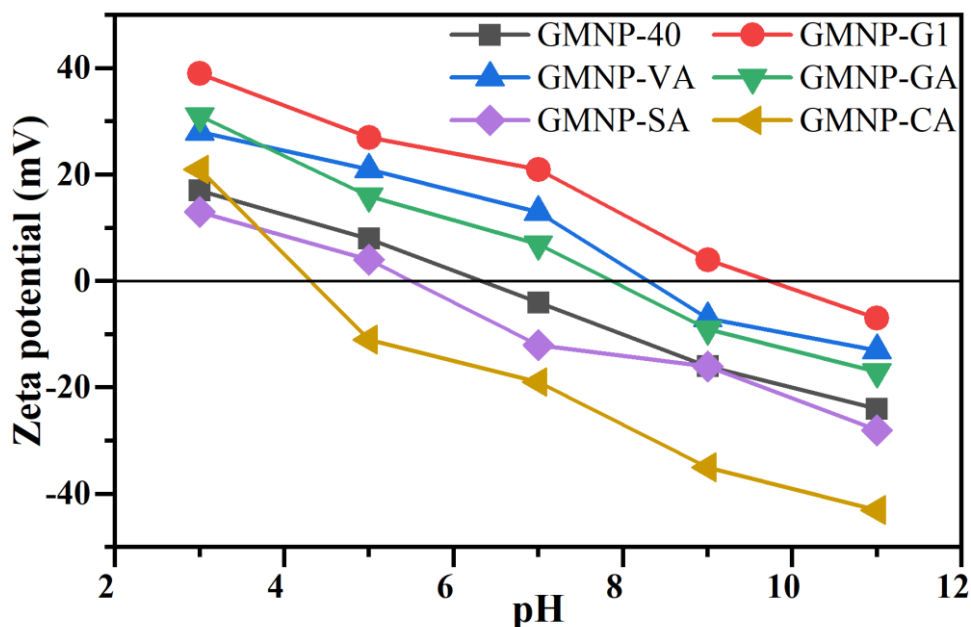


Figure 10: Zeta potential of GMNP-40, GMNP-G1, GMNP-VA, GMNP-CA, GMNP-SA, and GMNP-GA

4.2.4. Effect of pH

The most optimal pH for Pb (II) removal was found by adsorption tests at five different pH values (pH = 3, 5, 7, 9, and 11), as indicated in Figure 11. Since pH can disrupt the adsorbate's speciation and the functional groups that exist on the surface of the adsorbent, it is crucial to take into account how pH affects adsorption studies. There are different forms of Pb (II) species that may be found, such as Pb (II) and Pb(OH)⁺ at low pH and by raising the pH above 6, Pb(OH)₃⁻ is the predominant metal ion (Bang Njenjock et al., 2023). The initial concentration of Pb (II) was 50 mg/L with an adsorbent dosage of 100 mg/L at 30°C. GMNP-CA shows the maximum removal of Pb (II) at pH = 5. At low pH negative active sites are present on GMNP-CA that can be confirmed from zeta potential which is -11 at pH = 5, protonation of Pb (II) compete to occupy the maximum removal. At pH = 3 and 7, GMNP-CA also shows the maximum removal of Pb (II). As a result, surface complexation controls the adsorption of Pb (II) instead of electrostatic repulsion. Other than GMNP-CA, all composites show the minimum removal which is attributed to electrostatic repulsion. At pH = 9 and 11,

GMNP-SA and GMNP-G1 show the highest percentage of removal but there is a slight difference in removal with comparison to other composites. The difference in removal is due to the presence of deprotonation of metal ions which repels the negative sites of composites.

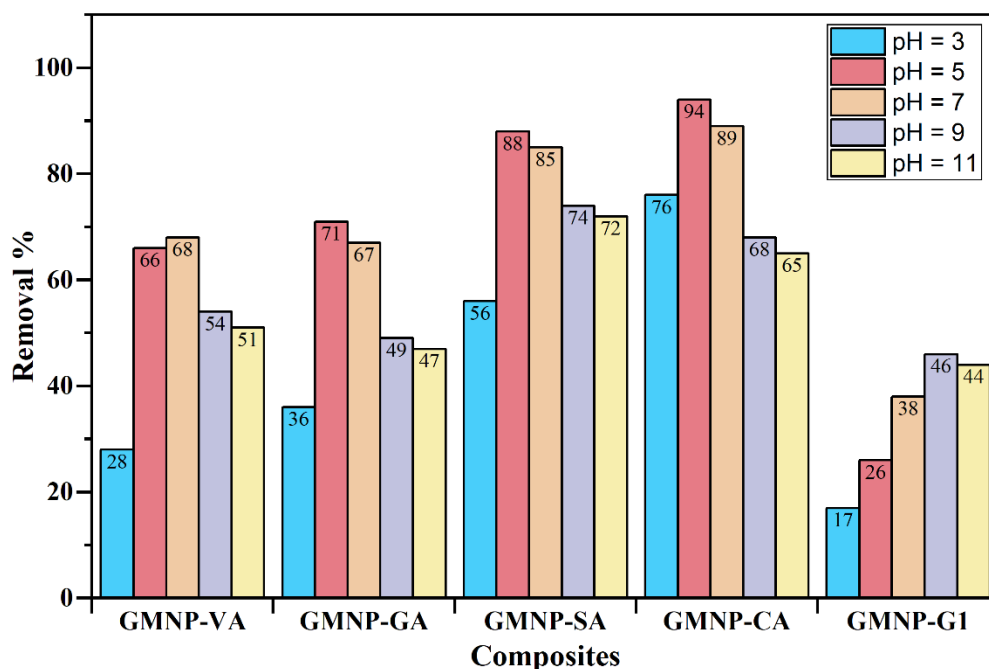


Figure 11: Effect of pH on Pb adsorption by GMNP-G1, GMNP-VA, GMNP-CA, GMNP-SA, and GMNP-GA

4.2.5. Effect of Initial Solution Concentration

Adsorption tests were conducted using GMNP-CA at initial concentrations ranging from 10 mg/L to 2200 mg/L in order to evaluate the impact on adsorption, as illustrated in Figure 12. With a pH of 5, an adsorbent dose of 100 mg/L, a contact time of 24 hours, and a temperature of 30°C. The removal percentage increases with increasing Pb (II) concentration, as shown in Figure. This maximum value of 600 mg/L is achieved with a removal efficiency of 92% and an adsorption capacity of 276.5 mg/g. As the starting concentration rises, the removal efficiency falls in tandem. At lower concentrations, there is a significant increase in the quantity of bulk adsorptive sites for binding and removal efficiency. Despite the fact that the early stages of the adsorption process result in saturated surface adsorption sites, the higher initial concentration leads to minimal bulk adsorptive sites.

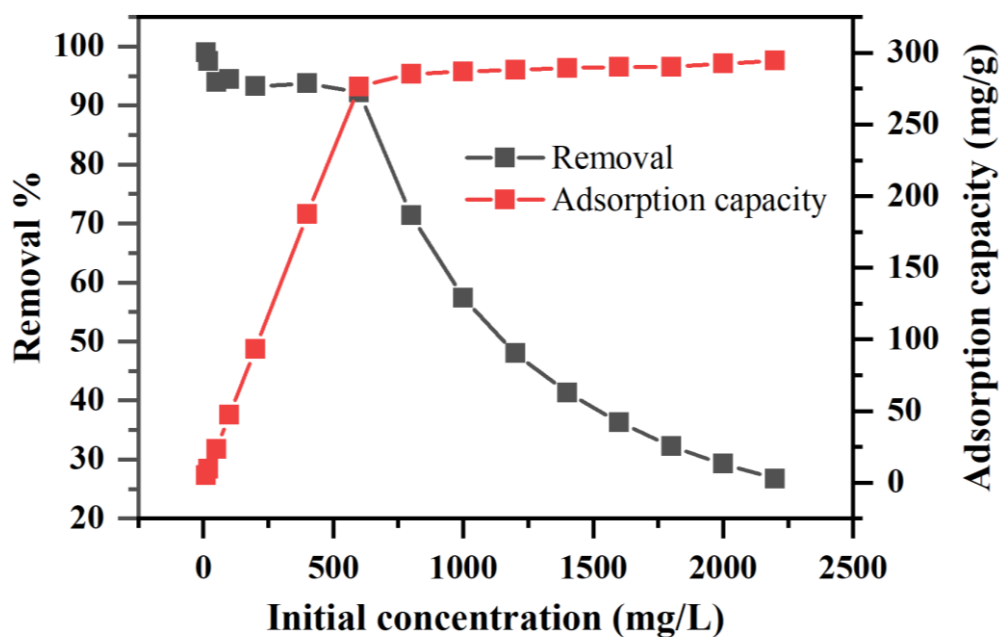


Figure 12: Effect of initial concentration for adsorption efficiency of GMNP-CA on Pb ions

4.2.6. Study of Contact Time

The repercussions of contact time to adsorption performance were accomplished by adjusting the experimental time ranging from 15 to 150 min. It is clear from Figure 13 that by increasing the time, removal efficiency was increasing. The optimum time found was 150 min. Keeping the pH = 5, adsorbent dosage = 100 mg/L and temperature = 30°C. In accordance with optimized conditions, the immobilization of MGO with functionalization augmented the removal efficiency. The stabilization was ensured with functionalization and dissuaded their agglomeration during the reaction between oxygenated groups and metal ions. The Pb (II) adsorption efficiency in this research shows promising results in comparison to other adsorbents used in previous studies.

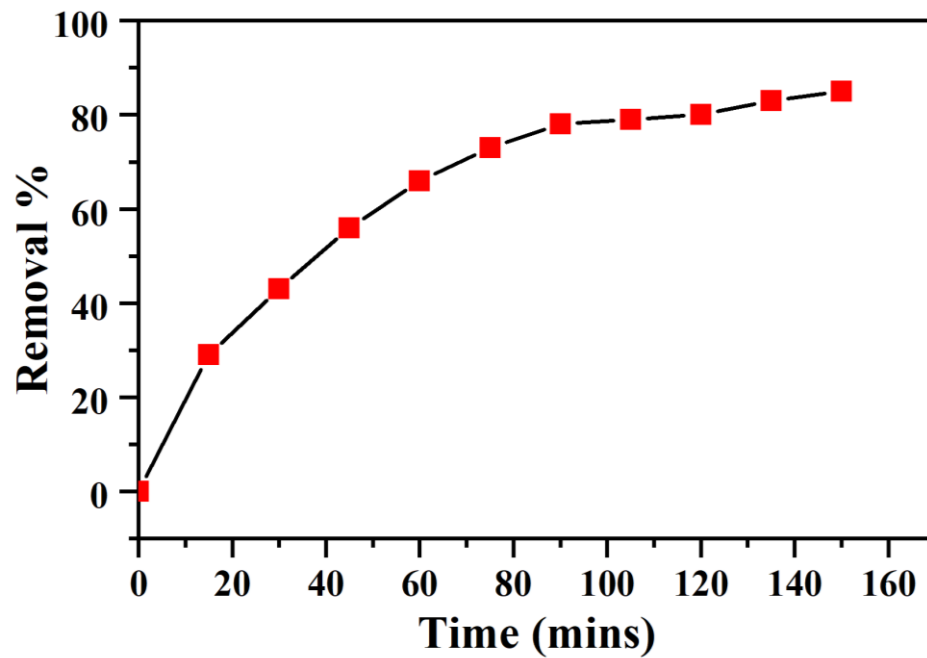


Figure 13: Effect of contact time for adsorption efficiency of GMNP-CA on Pb ions

4.2.7. Influence of Temperature

The efficacy of adsorption was realized by altering the five different temperatures (293K, 298K, 303K, 308K, and 313K). Holding the adsorption test for 24 h while maintaining the pH at 5 with 50 mg/L initial concentration of Pb (II) and 100 mg/L adsorbent dosage. Figure 14 demonstrated that the removal capability of composite increased by increasing the temperature that demonstrates the endothermic nature. Notably, after increasing the temperature from 308K to 313K, the removal becomes deficient. GMNP-CA shows the best results from overall composites with 97% removal at 308K.

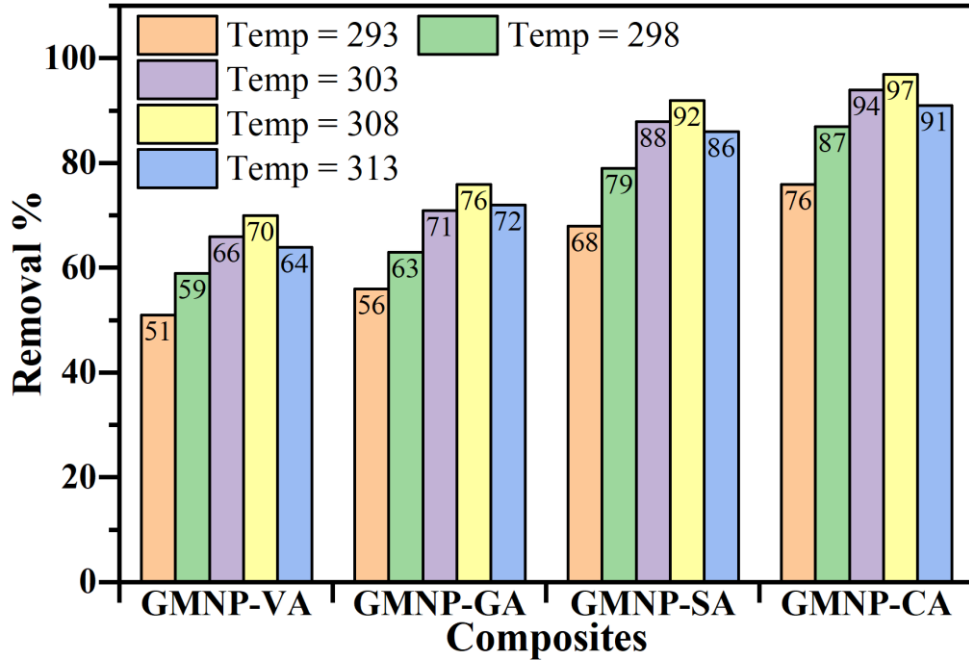


Figure 14: Effect of Temperature on Pb adsorption by GMNP-VA, GMNP-CA, GMNP-SA, and GMNP-GA

4.2.8. Isotherm Models

Adsorption isotherms are mathematical representations that shed light on how different adsorbate species are distributed between liquid and adsorbent. These models are based on conjectures regarding the type of coverage, possible interactions between adsorbate species, and the heterogeneity or homogeneity of the adsorbent. The interpretation of adsorption data by GMNP-CA is done using commonly used isotherms, like the Freundlich and Langmuir isotherms which are represented by equations 3 and 4 respectively. These isotherms provide a connection between the equilibrium material concentration in the bulk fluid phase (C_e) and the metal uptake per unit amount of adsorbent (Q_e) (Mahyoub et al., 2022).

$$\frac{1}{Q_e} = \frac{1}{K_L \times Q_{max}} \times \frac{1}{C_e} + \frac{1}{Q_{max}} \quad (3)$$

$$\log Q_e = \log K_f + \frac{1}{n} \log C_e \quad (4)$$

C_e represents the metal ion equilibrium concentration (mg/L), K_L is the Langmuir adsorption constant, which is correlated with adsorption energy (L/g), Q_{max} is the maximum amount of metal that can be adsorbed onto an adsorbent (mg/g), and Q_e is

the amount of Pb (II) that can be adsorbed onto an adsorbent at equilibrium (mg/g). Freundlich constant (K_F) is a measure of the adsorbent's relative adsorption capacity (L/g) and the slope of $1/n$ shows how concentration affects this capacity and provides information on adsorption intensity. A value of 1 denotes that there is no concentration in the division between the two phases. A standard adsorption is shown if the value of $1/n$ is less than one. As opposed to this, cooperative adsorption is shown if the value of $1/n$ is greater than 1. Table 2 lists the variables used in isotherms of adsorption models.

Table 2: Parameters of the isotherm models for the sorption of Pb

Material	Langmuir			Freundlich		
	Q _m (mg/g)	K _L (L/g)	R ²	1/n	K _F (L/g)	R ²
GMNP-CA	16.47	18.01	0.9997	0.32072	4.752069	0.75669

The monolayer adsorption hypothesis has been bolstered by the Langmuir model's superior fit to the Pb adsorption over the Freundlich model in Figure 15. The adsorption capacity of Pb (II) on GMNP-CA was 16.47 mg/g, it was imputable to one hydroxyl and two carboxyl groups pursuant branch, which ardently participated in Pb (II) adsorption. Pb (II) had higher R² value of 0.9997 for the Langmuir model. The amine functional groups on GMNP-CA are more appropriate to be favored by Pb (II) due to their higher Pauling electro negativity of 1.87, which in turn causes a stronger attraction to isolated electron pairs in donor atoms and the formation of more stable complexes. (Alves Macedo et al., 2021). Further indications that Pb (II) is more seamlessly adsorbed through sorption reactions or surface complexations come from the fact that Pb (II) has a lower pK_H (Hydrolysis constant's negative log = 7.71). Additionally, the different adsorption inclinations for Pb (II) onto the GMNP-CA can also be interpreted as Pb (II) having a larger ionic radius (1.21) and higher Misono softness value (3.58) (Miranda et al., 2022).

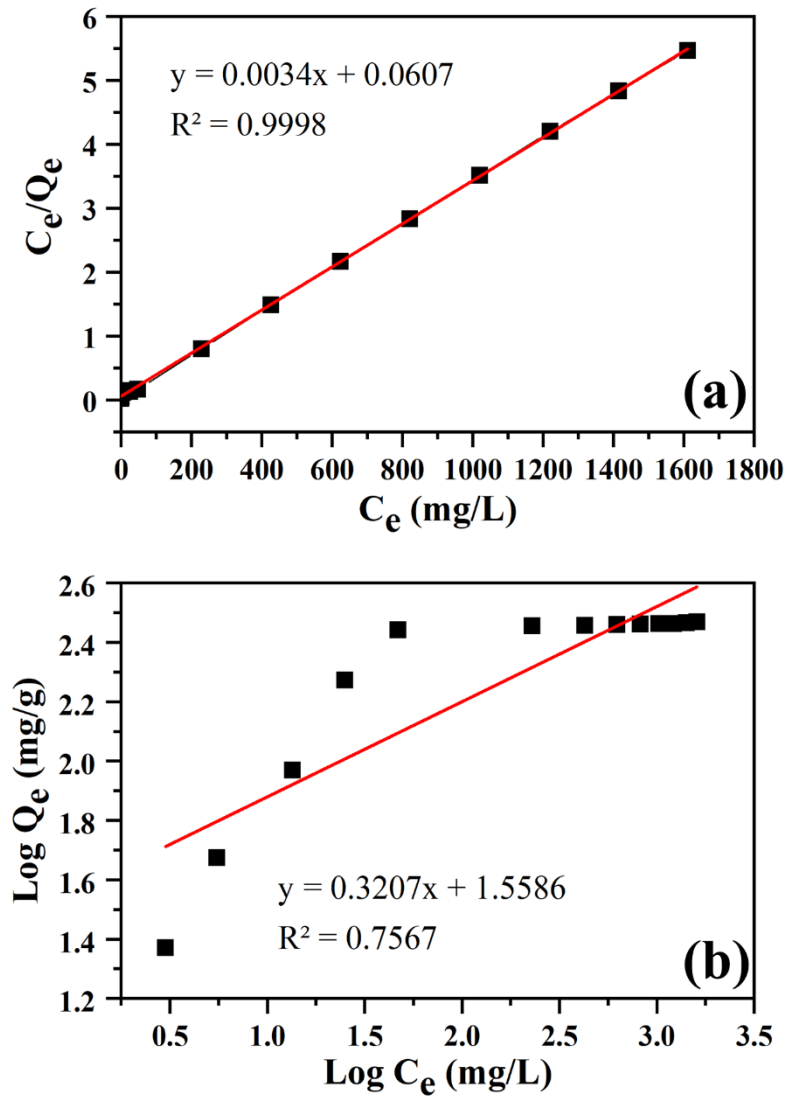


Figure 15: (a) Langmuir model and (b) Freundlich model for the adsorption of Pb ions on GMNP-CA

4.2.9. Kinetic Models

In order to understand the mechanism of Pb adsorption and evaluate the effectiveness of adsorbents for Pb removal, kinetic models are indispensable. These models follow rate laws, which means that a thorough comprehension of the specific molecular steps, interatomic distances, and chemical reactions are required. Examining the amount of Pb still present in the liquid state at equilibrium time is the simplest method for interpreting data from a batch kinetic study. The adsorption data from GMNP-CA are interpreted using two widely used kinetic models, pseudo first order (PFO) and pseudo second order (PSO), represented by equations 5 and 6 (Jaber et al., 2022).

$$\ln(q_e - qt) = \ln q_e - K_1 t \quad (5)$$

$$\frac{t}{q_e} = \frac{1}{K_2 q_e^2} + \frac{1}{q_e} \quad (6)$$

where t is a variable time interval (mins), K₁ and K₂ are rate constants (/min), and Q_e is the amount of Pb (II) adsorption onto adsorbent at equilibrium (mg/g). Q_t is the intake of Pb (II) at the span of time (mg/g). Table 3 lists the variables used in the kinetics of adsorption models.

Table 3: Parameters of the kinetic models for the sorption of pb

Material	Pseudo first order			Pseudo second order		
	Q (mg/g)	K ₁ (/min)	R ²	Q (mg/g)	K ₂ (/min)	R ²
GMNP-CA	19.53817	-0.000101	0.9953	4.566011	0.000243	0.9720

PFO model reliably foretold the best-fitted model then PSO for the adsorption kinetics (R²=0.99) as shown in figure 16. The kinetic model fitting had been anticipated that the adsorption between GMNP-CA and Pb (II) is subsequently physical adsorption that could be ascribed to electrostatic attraction, hydrogen bonding, and ionic adsorption. In PFO kinetics, a higher value of Q indicates that the adsorption process is more in line with a first-order reaction. The concentration of the adsorbate on the adsorbent surface in this case largely determines the rate of adsorption as well. The initial adsorption rate is high due to the quickly occupied adsorption sites, but it may eventually fall.

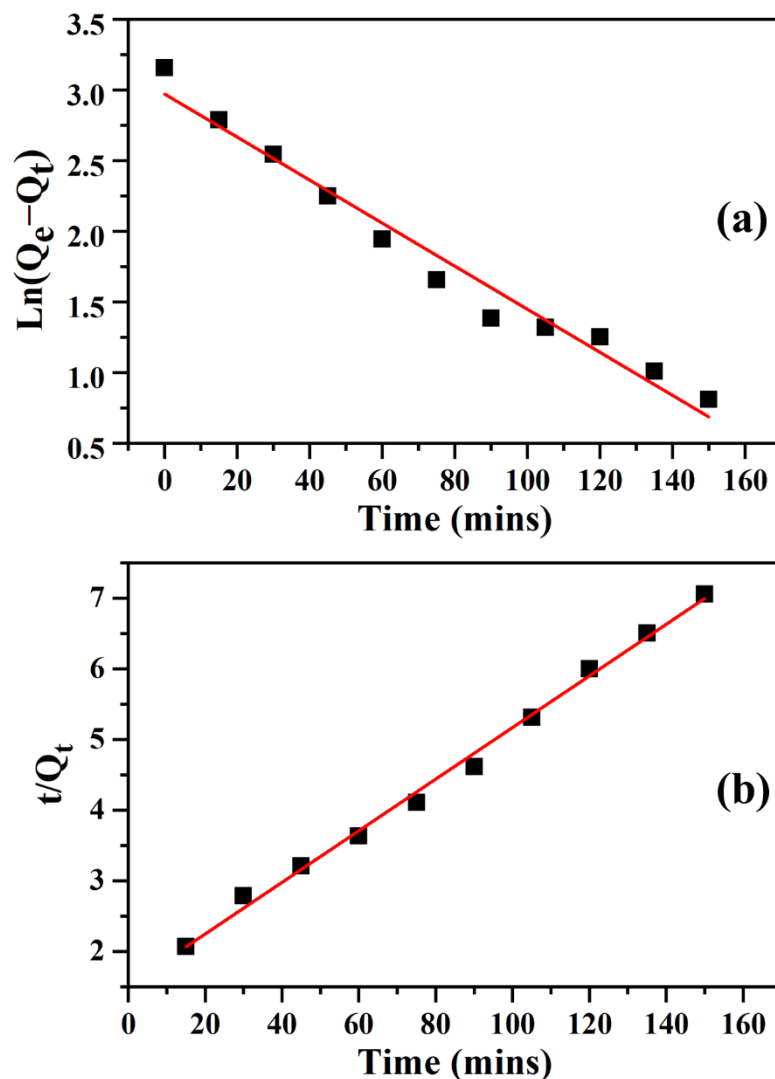


Figure 16: (a) pseudo first order and (b) pseudo second order for the adsorption of Pb ions on GMNP-CA

4.3. Regeneration

Reusability is essential for prominent adsorbents to ensure that it makes them economical and environmentally friendly. The cyclic adsorption-desorption experiments were performed in ten cycles to evaluate the reusability potential of the nanomaterial (Mehdinia et al., 2020). Composite retrieved through magnetic separation adhering to each experiment. After dispersing in a 30 mL solution of 10^{-3} M HCl and stirring for one hour, the composite was desorption from it. A subsequent adsorption experiment was conducted on the regenerated composite after it had been cleaned with deionized water. Figure 17 shows the on-fleek 90% adsorption removal of Pb (II) by GMNP-CA up to 10 cycles. Applications associated with large-scale water treatment

reap the benefits from Gargantuan's sustainable efficacy and brevity in severance from contaminated water. Withal the biocompatibility of groups in organic acids fosters thwarting the eco-toxicological ramifications of nanomaterials for ameliorated environment and human health.

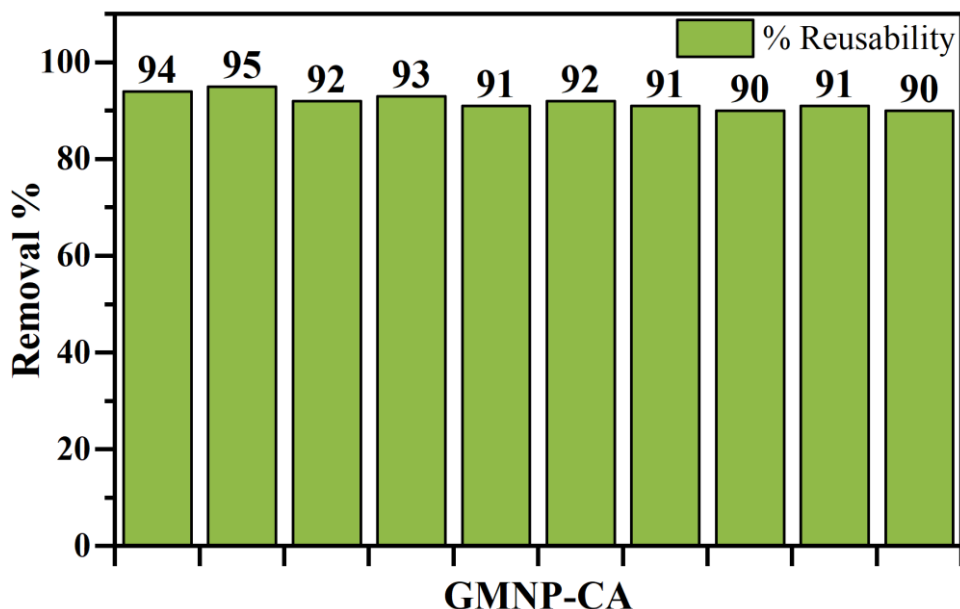


Figure 17: Regeneration of GMNP-CA for Pb adsorption

4.4. Contaminant Comparison with Literature Studies

The Pb (II) sorption capacity using various sorbents that have been reported in earlier studies is compared in Table 4. Water chemistry parameters and adsorbent type showed a strong correlation with Pb (II) adsorption capacity across a range of aqueous matrices.

Table 4: Comparing the latest prepared nanocomposites' performance in removing Pb

Composite	Lead Conc. (ppm)	Removal %	Adsorption capacity (mg/g)	Equ. adsorption time (min)	pH	Dosage (mg/L)	Reference
Porous carbon nanofibers (PCNFs)	10	79	7.1	1	7	200	(Mahar et al., 2019)
Graphene oxide	500	99.9	500	60	9	66.6	(Rashida & Abdul, 2020)
Dopamine polymerization in MOFs	0.150	99.35	7.18	10	6.5	66.6	(Y. Zhang et al., 2021)

Amino functionalized Ti ₃ C ₂ T _x MXene	25	100	385	30	6.3	500	(G. Zhang et al., 2020)
MXene alginate composites	48	86.7	383	15	6	1000	(Dong, 2019)
Partially reduced graphene oxide Fe ₃ O ₄	97.68	95.77	373.14	10	6	250	(Li, 2018)
MnO ₂ gelatin	100	92	318.7	240	6	500	(X. Wang et al., 2018)
Cellulose manganese dioxide	100	99.95	290.8	120	6	500	(Fu & Xie, 2020)
SiO ₂ MgO hybrid fibers (SMHFs)	100	98	787.9	30	6	333.3	(Xu et al., 2020)
Polyaniline Fe ₃ O ₄ silver diethyldithiocarbamate (PANIFS)	45	94	40.3	45	6	111.1	(Hashemi et al., 2019)
clinoptilolite	50	96.3	47.4	90	6	50	(Heidarian et al., 2023)
3-phenyl-1(2-pyridyl) thiourea (PPTU)	200	98.2	57.1	90	5	4800	(Şanlıer Uçak & Aydın, 2022)
GMNP-CA	600	94	276.5	150	5	100	This study

CONCLUSION AND RECOMMENDATIONS

5.1. Conclusion

As a new biosorbent that can remove Pb (II) ions from water, the feasibility of GMNP-CA was thoroughly investigated. The following are the main conclusions reached by the current study:

- In this study, GO and MNPs were successfully synthesized using Modified Hummer's method and co-precipitation method respectively. Afterward, GMNPs with different percentage ratios (70 to 20) were synthesized.
- GMNP-40 was chosen for further modification because it shows comparable results with other composites. The dendritic structure was effectively anchored on GMNP-40 which forms GMNP-G1.
- Then CA, GA, SA, and VA were fabricated on GMNP-G1 which shows excellent stability and magnetic separation, it also increases the number of branches for adsorptive sites. There is a nominal effect of functionalization on the morphology of composites.
- GMNP-CA achieved an adsorption capacity of 276.5 mg/g with a 94% removal of Pb, observed at a pH of 5 while utilizing 100 mg/L of adsorbent.
- Overall, GMNP-CA is the highest removal adsorbent, which is ascribed to monolayer and physical adsorption through electrostatic attraction, hydrogen bonding, and ionic adsorption. It is not subjected to any physical changes and can be reused for up to ten cycles with nearly the same removal efficiency.
- In summary, dendrimer and acid-based functionalization of GO reflect promise for extensive use in the water treatment industry due to their effective Pb (II) removal, biocompatibility and reusability.

5.2. Recommendations

This study recommends that:

- The adsorption potential of GMNP-GA and GMNP-VA having aromatic functional groups should be assessed for the removal of non-polar contaminants from water.
- Future research and development could focus on the creation of a scalable and economically feasible synthesis method for GO.
- Investigate the effect of higher generation of dendrimers (G2, G3, G4, and G5) on the removal of Pb from aqueous solution.

REFERENCES

- Ahmad, S. Z. N., Wan Salleh, W. N., Ismail, A. F., Yusof, N., Mohd Yusop, M. Z., & Aziz, F. (2020). Adsorptive removal of heavy metal ions using graphene-based nanomaterials: Toxicity, roles of functional groups and mechanisms. *Chemosphere*, *248*, 126008. <https://doi.org/10.1016/j.chemosphere.2020.126008>
- Al-Qahtani, K. M. (2017). Cadmium removal from aqueous solution by green synthesis zero valent silver nanoparticles with Benjamina leaves extract. *Egyptian Journal of Aquatic Research*, *43*(4), 269–274. <https://doi.org/10.1016/j.ejar.2017.10.003>
- Albert, E. L., Che Abdullah, C. A., & Shiroshaki, Y. (2018). Synthesis and characterization of graphene oxide functionalized with magnetic nanoparticle via simple emulsion method. *Results in Physics*, *11*(October), 944–950. <https://doi.org/10.1016/j.rinp.2018.10.054>
- Alves Macedo, J. C., Sartori Jeunon Gontijo, E., Gómez Herrera, S., Rangel, E. C., Komatsu, D., Landers, R., & Rosa, A. H. (2021). Organosulphur-modified biochar: An effective green adsorbent for removing metal species in aquatic systems. *Surfaces and Interfaces*, *22*(October 2020). <https://doi.org/10.1016/j.surfin.2020.100822>
- Azadmanjiri, J., Berndt, C. C., Wang, J., Kapoor, A., & Srivastava, V. K. (2016). Nanolaminated composite materials: Structure, interface role and applications. *RSC Advances*, *6*(111), 109361–109385. <https://doi.org/10.1039/c6ra20050h>
- Bacha, K., Chemotti, C., Mbakidi, J., & Deleu, M. (2023). *Dendrimers : Synthesis , Encapsulation Applications and Specific Interaction with the Stratum Corneum — A Review*. 343–370.
- Bang Njenjock, B. B., Thiodjio Sendja, B., Tchana Kamgne, D., Medellin Castillo, N. A., Loredó Portales, R., Labrada Delgado, G. J., Aquilanti, G., & Ben-Bolie, G. H. (2023). Lead sorbed onto volcanic ashes investigated by x-ray absorption spectroscopy and complementary techniques. *Journal of Electron Spectroscopy and Related Phenomena*, *262*(November 2022), 147268. <https://doi.org/10.1016/j.elspec.2022.147268>
- Barkade, S., Sable, S., Ashtekar, V., & Pandit, V. (2022). Removal of lead and copper from wastewater using Bael fruit shell as an adsorbent. *Materials Today:*

Proceedings, 53, 65–70. <https://doi.org/10.1016/j.matpr.2021.12.300>

- Boeykens, S. P., Redondo, N., Obeso, R. A., Caracciolo, N., & Vázquez, C. (2019). Chromium and Lead adsorption by avocado seed biomass study through the use of Total Reflection X-Ray Fluorescence analysis. *Applied Radiation and Isotopes*, 153(July), 108809. <https://doi.org/10.1016/j.apradiso.2019.108809>
- Briffa, J., Sinagra, E., & Blundell, R. (2020). Heliyon Heavy metal pollution in the environment and their toxicological effects on humans. *Heliyon*, 6(September 2019), e04691. <https://doi.org/10.1016/j.heliyon.2020.e04691>
- Bulin, C., Zheng, R., Song, J., Bao, J., Xin, G., & Zhang, B. (2023). Magnetic graphene oxide-chitosan nanohybrid for efficient removal of aqueous Hg(II) and the interaction mechanism. *Journal of Molecular Liquids*, 370, 121050. <https://doi.org/10.1016/j.molliq.2022.121050>
- Chandio, T. A., Khan, M. N., Muhammad, M. T., Yalcinkaya, O., & Kayis, A. F. (2020). Co-exposure of neurotoxic contaminants (Pb and Mn) in drinking water of Zhob District, Baluchistan Pakistan. *Environmental Nanotechnology, Monitoring and Management*, 14, 100328. <https://doi.org/10.1016/j.enmm.2020.100328>
- Chen, Y., Wang, B., & Hou, W. (2021). Chemosphere Graphitic carbon nitride embedded with graphene materials towards photocatalysis of bisphenol A : The role of graphene and mediation of superoxide and singlet oxygen. *Chemosphere*, 278, 130334. <https://doi.org/10.1016/j.chemosphere.2021.130334>
- Cheng, J., Gao, M., Yang, L., Zhang, L., & Zhu, B. (2020). Coral-inspired “nanotentaclization” porous composite gel for efficient removal of Lead (II) from aqueous solution. *Materials & Design*, 195, 109072. <https://doi.org/10.1016/j.matdes.2020.109072>
- Daud, M. K., Nafees, M., Ali, S., Rizwan, M., Bajwa, R. A., Shakoor, M. B., Arshad, M. U., Chatha, S. A. S., Deeba, F., Murad, W., Malook, I., & Zhu, S. J. (2017). Drinking Water Quality Status and Contamination in Pakistan. *BioMed Research International*, 2017. <https://doi.org/10.1155/2017/7908183>
- Du, B., Chai, L., Li, W., Wang, X., Chen, X., Zhou, J., & Sun, R. C. (2022). Preparation of functionalized magnetic graphene oxide/lignin composite nanoparticles for

- adsorption of heavy metal ions and reuse as electromagnetic wave absorbers. *Separation and Purification Technology*, 297(April), 121509. <https://doi.org/10.1016/j.seppur.2022.121509>
- Fu, B., & Xie, F. (2020). Facile in situ synthesis of cellulose microcrystalline-manganese dioxide nanocomposite for effective removal of Pb(II) and Cd(II) from water. *Environmental Science and Pollution Research*, 27(5), 5108–5121. <https://doi.org/10.1007/s11356-019-07159-7>
- Gaur, S., Singh, N., & Saxena, S. (2011). Status of lead present in ground drinking water samples of Uttarakhand (Garhwal Region) in India . *Asian Journal of Biomedical and Pharmaceutical Sciences*, 1(1), 32–38.
- Gayen, S., Bej, B., Boxi, S. S., & Ghosh, R. (2023). Materials Today : Proceedings Synthesis of graphene oxide and its application for purification of river water. *Materials Today: Proceedings*, 72, 2630–2636. <https://doi.org/10.1016/j.matpr.2022.08.131>
- Ge, X., Su, G., Che, W., Yang, J., Zhou, X., Wang, Z., Qu, Y., Yao, T., Liu, W., & Wu, Y. (2020). Atomic Filtration by Graphene Oxide Membranes to Access Atomically Dispersed Single Atom Catalysts. <https://doi.org/10.1021/acscatal.0c02203>
- Geng, X., Qu, R., Kong, X., Geng, S., & Zhang, Y. (2021). Facile Synthesis of Cross-linked Hyperbranched Polyamidoamines Dendrimers for Efficient Hg (II) Removal From Water. 9(September), 1–14. <https://doi.org/10.3389/fchem.2021.743429>
- Hashemi, S. A., Mousavi, S. M., & Ramakrishna, S. (2019). Effective removal of mercury, arsenic and lead from aqueous media using Polyaniline-Fe₃O₄- silver diethyldithiocarbamate nanostructures. *Journal of Cleaner Production*, 239, 118023. <https://doi.org/10.1016/j.jclepro.2019.118023>
- Heidari, Y., Noroozian, E., & Maghsoudi, S. (2023). Improvement of salt rejection efficiency of cellulose acetate membrane through modification by poly(amidoamine) dendrimer-functionalized graphene oxide. *Heliyon*, 9(9), e19171. <https://doi.org/10.1016/j.heliyon.2023.e19171>
- Heidarian, M. H., Nakhaei, M., Vatanpour, V., & Rezaei, K. (2023). Evaluation of

- using clinoptilolite as a filter in drinking water wells for removal of lead (small-scale physical sand box model). *Journal of Water Process Engineering*, 52(February), 103558. <https://doi.org/10.1016/j.jwpe.2023.103558>
- Hosseini, S. M., Jashni, E., Habibi, M., & Bruggen, B. Van Der. (2018). *Fabrication of novel electro dialysis heterogeneous ion exchange membranes by incorporating PANI / GO functionalized composite nanoplates*. 1789–1801.
- Hube, S., Eska, M., Hrafnkelsdóttir, K. F., Bjarnadóttir, B., Bjarnadóttir, M. Á., Axelsdóttir, S., & Wu, B. (2020). *Science of the Total Environment Direct membrane filtration for wastewater treatment and resource recovery : A review*. 710. <https://doi.org/10.1016/j.scitotenv.2019.136375>
- Israr, M., Iqbal, J., Arshad, A., Rani, M., Romero, P. G., & Benages, R. (2020). Graphene triggered enhancement in visible-light active photocatalysis as well as in energy storage capacity of (CFO) 1-x (GNPs) x nanocomposites. *Ceramics International*, 46(3), 2630–2639. <https://doi.org/10.1016/j.ceramint.2019.09.232>
- Jaber, L., Ihsanullah, I., Almanassra, I. W., Backer, S. N., Abushawish, A., Khalil, A. K. A., Alawadhi, H., Shanableh, A., & Atieh, M. A. (2022). Adsorptive Removal of Lead and Chromate Ions from Water by Using Iron-Doped Granular Activated Carbon Obtained from Coconut Shells. *Sustainability (Switzerland)*, 14(17), 1–24. <https://doi.org/10.3390/su141710877>
- Järup, L. (2003). *Hazards of heavy metal contamination*. 68, 167–182. <https://doi.org/10.1093/bmb/ldg032>
- Javid, S., Shah, S. G. S., Chaudhary, A. J., & Khan, M. H. (2008). Assessment of trace metal contamination of drinking water in the Pearl Valley, Azad Jammu and Kashmir. *Clean - Soil, Air, Water*, 36(2), 216–221. <https://doi.org/10.1002/clen.200700055>
- Jimenez-Cervantes, E., López-Barroso, J., Martínez-Hernández, A. L., & Velasco-Santos, C. (2016). Graphene-Based Materials Functionalization with Natural Polymeric Biomolecules. *Recent Advances in Graphene Research*. <https://doi.org/10.5772/64001>
- Kim, H. K., Anwer, H., & Park, J. W. (2022). Citric, succinic, and vanillic acid-

- functionalized magnetic-cored dendrimer for methylene blue adsorption. *Journal of Environmental Science and Health - Part A Toxic/Hazardous Substances and Environmental Engineering*, 57(10), 902–912. <https://doi.org/10.1080/10934529.2022.2130646>
- Kim, H., Park, J., Kim, H., & Park, J. (2019). Toxic / Hazardous Substances and Environmental Engineering Agglomeration of 10 nm amine-functionalized nano-magnetite does not hinder its efficiency as an environmental adsorbent its efficiency as an environmental adsorbent. *Journal of Environmental Science and Health, Part A*, 0(0), 1–9. <https://doi.org/10.1080/10934529.2019.1579535>
- Kim, K. J., & Park, J. W. (2017). Stability and reusability of amine-functionalized magnetic-cored dendrimer for heavy metal adsorption. *Journal of Materials Science*, 52(2), 843–857. <https://doi.org/10.1007/s10853-016-0380-z>
- Krishna, R. H., Chandraprabha, M. N., Samrat, K., Krishna Murthy, T. P., Manjunatha, C., & Kumar, S. G. (2023). Carbon nanotubes and graphene-based materials for adsorptive removal of metal ions – A review on surface functionalization and related adsorption mechanism. *Applied Surface Science Advances*, 16(June), 100431. <https://doi.org/10.1016/j.apsadv.2023.100431>
- Kuang, Y., Zhang, Z., & Wu, D. (2022). Synthesis of graphene oxide/polyethyleneimine sponge and its performance in the sustainable removal of Cu(II) from water. *Science of the Total Environment*, 806, 151258. <https://doi.org/10.1016/j.scitotenv.2021.151258>
- Kumar, V., & Dwivedi, S. K. (2021). Bioremediation mechanism and potential of copper by actively growing fungus *Trichoderma lixii* CR700 isolated from electroplating wastewater. *Journal of Environmental Management*, 277(August 2020), 111370. <https://doi.org/10.1016/j.jenvman.2020.111370>
- Levchuk, I., Fern, P., Sillanp, M., & Jos, J. (2020). *A critical review on application of photocatalysis for toxicity reduction of real wastewaters*. 258. <https://doi.org/10.1016/j.jclepro.2020.120694>
- Li, B. (2018). *Efficient removal of aqueous Pb (II) using partially reduced. Ii*. <https://doi.org/10.1177/0263617417744402>

- Liu, W.-X., Song, S., Ye, M.-L., Zhu, Y., Zhao, Y.-G., & Lu, Y. (2022). Nanomaterials with Excellent Adsorption Characteristics for Sample Pretreatment: A Review. *Nanomaterials*, *12*(11), 1845. <https://doi.org/10.3390/nano12111845>
- Lyu, Z., Ding, L., Huang, A. Y., Kao, C., & Peng, L. (2019). Poly (amidoamine) dendrimers : covalent and supramolecular synthesis. *Materials Today Chemistry*, *13*, 34–48. <https://doi.org/10.1016/j.mtchem.2019.04.004>
- Mahar, F. K., He, L., Wei, K., Mehdi, M., Zhu, M., Gu, J., Zhang, K., Khatri, Z., & Kim, I. (2019). Rapid adsorption of lead ions using porous carbon nanofibers. *Chemosphere*, *225*, 360–367. <https://doi.org/10.1016/j.chemosphere.2019.02.131>
- Mahyoob, W., Alakayleh, Z., Abu Hajar, H. A., Al-Mawla, L., Altwaiq, A. M., Al-Remawi, M., & Al-Akayleh, F. (2022). A novel co-processed olive tree leaves biomass for lead adsorption from contaminated water. *Journal of Contaminant Hydrology*, *248*(May), 104025. <https://doi.org/10.1016/j.jconhyd.2022.104025>
- Manual, P. (n.d.). *Heavy Metal Testing*.
- Manzoor, S., Shah, M. H., Shaheen, N., Khaliq, A., & Jaffar, M. (2006). Multivariate analysis of trace metals in textile effluents in relation to soil and groundwater. *Journal of Hazardous Materials*, *137*(1), 31–37. <https://doi.org/10.1016/j.jhazmat.2006.01.077>
- Mehdinia, A., Heydari, S., & Jabbari, A. (2020). Synthesis and characterization of reduced graphene oxide-Fe₃O₄@polydopamine and application for adsorption of lead ions: Isotherm and kinetic studies. *Materials Chemistry and Physics*, *239*(August 2019), 121964. <https://doi.org/10.1016/j.matchemphys.2019.121964>
- Miranda, L. S., Ayoko, G. A., Egodawatta, P., & Goonetilleke, A. (2022). Adsorption-desorption behavior of heavy metals in aquatic environments: Influence of sediment, water and metal ionic properties. *Journal of Hazardous Materials*, *421*(July 2021), 126743. <https://doi.org/10.1016/j.jhazmat.2021.126743>
- Nasir, S., Hussein, M. Z., Zainal, Z., & Yusof, N. A. (2018). Carbon-based nanomaterials/allotropes: A glimpse of their synthesis, properties and some applications. *Materials*, *11*(2), 1–24. <https://doi.org/10.3390/ma11020295>
- Natasha, N., Dumat, C., Shahid, M., & Khalid, S. (2020). *Metadata of the chapter that*

will be visualized online (Issue October 2021). <https://doi.org/10.1007/978-3-030-21638-2>

- Ndlwana, L., Motsa, M. M., & Mamba, B. B. (2020). A unique method for dopamine-cross-linked graphene nanoplatelets within polyethersulfone membranes (GNP-pDA / PES) for enhanced mechanochemical resistance during NF and RO desalination. *European Polymer Journal*, 136(July), 109889. <https://doi.org/10.1016/j.eurpolymj.2020.109889>
- Nemati, M., Hosseini, S. M., & Shabanian, M. (2017). Novel electro dialysis cation exchange membrane prepared by 2-acrylamido-2-methylpropane sulfonic acid ; heavy metal ions removal. *Journal of Hazardous Materials*, 337, 90–104. <https://doi.org/10.1016/j.jhazmat.2017.04.074>
- Neolaka, Y. A. B., Lawa, Y., Naat, J. N., Riwu, A. A. P., Iqbal, M., Darmokoesoemo, H., & Kusuma, H. S. (2020). The adsorption of Cr(VI) from water samples using graphene oxide-magnetic (GO-Fe₃O₄) synthesized from natural cellulose-based graphite (kusambi wood or *Schleichera oleosa*): Study of kinetics, isotherms and thermodynamics. *Journal of Materials Research and Technology*, 9(3), 6544–6556. <https://doi.org/10.1016/j.jmrt.2020.04.040>
- Pabbati, R., Kondakindi, V. R., & Shaik, F. (2021). *Applications of Nanomaterials in Biomedical Engineering* (Issue March). https://doi.org/10.1007/978-981-15-9916-3_3
- Peiman, S., Baharfar, R., & Maleki, B. (2021). Immobilization of trypsin onto polyamidoamine dendrimer functionalized iron oxide nanoparticles and its catalytic behavior towards spirooxindole-pyran derivatives in aqueous media. *Materials Today Communications*, 26(September 2020), 101759. <https://doi.org/10.1016/j.mtcomm.2020.101759>
- Pronk, W., Ding, A., Morgenroth, E., Derlon, N., Desmond, P., Burkhardt, M., Wu, B., & Fane, A. G. (2019). Gravity-driven membrane filtration for water and wastewater treatment : A review. *Water Research*, 149, 553–565. <https://doi.org/10.1016/j.watres.2018.11.062>
- Qasem, N. A. A., Mohammed, R. H., & Lawal, D. U. (2021). Removal of heavy metal ions from wastewater: a comprehensive and critical review. *Npj Clean Water*, 4(1).

<https://doi.org/10.1038/s41545-021-00127-0>

- Rashida, N., & Abdul, N. (2020). *Adsorption studies of graphene oxide for lead removal from adsorption studies of graphene oxide for lead removal from synthetic wastewater. January.*
- Rizwan, U., Malik, R. N., & Abdul, Q. (2009). Assessment of groundwater contamination in an industrial city, Sialkot, Pakistan. *African Journal of Environmental Science and Technology*, 3(12), 429–446. http://www.academicjournals.org/ajest/PDF/pdf_2009/Dec/Ullah_et_al.pdf%5Cnhttp://ovidsp.ovid.com/ovidweb.cgi?T=JS&CSC=Y&NEWS=N&PAGE=fulltext&D=cagh&AN=20103317248%5Cnhttp://lshtmsfx.hosted.exlibrisgroup.com/lshtm?sid=OVID:caghdb&id=pmid:&id=doi:&issn=1996
- Rudrapati, R. (2020). Graphene: Fabrication Methods, Properties, and Applications in Modern Industries. *Graphene Production and Application*, 1–14. <https://doi.org/10.5772/intechopen.92258>
- Şanlıer Uçak, Ş., & Aydın, A. (2022). A novel thiourea derivative for preconcentration of copper(II), nickel(II), cadmium(II), lead(II) and iron(II) from seawater samples for Flame Atomic Absorption Spectrophotometry. *Marine Pollution Bulletin*, 180(January). <https://doi.org/10.1016/j.marpolbul.2022.113787>
- Serol, A., & Gökhan, E. (2018). PAMAM Dendrimer Functionalized Manganese Ferrite Magnetic Nanoparticles: Microwave-Assisted Synthesis and Characterization. *Journal of Inorganic and Organometallic Polymers and Materials*, 28(5), 2100–2107. <https://doi.org/10.1007/s10904-018-0865-0>
- Shahzad, A., Nawaz, M., Moztahida, M., Jang, J., Tahir, K., & Kim, J. (n.d.). *Ti₃C₂Tx MXene core-shell spheres for ultrahigh removal of mercuric ions.*
- Singh, S., Anil, A. G., Khasnabis, S., Kumar, V., Nath, B., Adiga, V., Kumar Naik, T. S. S., Subramanian, S., Kumar, V., Singh, J., & Ramamurthy, P. C. (2022). Sustainable removal of Cr(VI) using graphene oxide-zinc oxide nanohybrid: Adsorption kinetics, isotherms and thermodynamics. *Environmental Research*, 203(June 2021). <https://doi.org/10.1016/j.envres.2021.111891>
- Tang, Y., Yang, C., & Que, W. (2018). A novel two-dimensional accordion-like

- titanium carbide (MXene) for adsorption of Cr(VI) from aqueous solution. *Journal of Advanced Dielectrics*, 8(5). <https://doi.org/10.1142/S2010135X18500352>
- Thabede, P. M., Shooto, N. D., & Naidoo, E. B. (2020). South African Journal of Chemical Engineering Removal of methylene blue dye and lead ions from aqueous solution using activated carbon from black cumin seeds. *South African Journal of Chemical Engineering*, 33(October 2019), 39–50. <https://doi.org/10.1016/j.sajce.2020.04.002>
- Thi Mong Thy, L., Tan Tai, L., Duy Hai, N., Quang Cong, C., Minh Dat, N., Ngoc Trinh, D., Truong Son, N., Thi Yen Oanh, D., Thanh Phong, M., & Huu Hieu, N. (2022). Comparison of in-situ and ex-situ methods for synthesis of iron magnetic nanoparticles-doped graphene oxide: Characterization, adsorption capacity, and Fenton catalytic efficiency. *FlatChem*, 33(March), 100365. <https://doi.org/10.1016/j.flatc.2022.100365>
- Tiwari, S., Prasad, I., Mahatma, T., Chitrakoot, G., Vishwavidyalaya, G., Tiwari, H., Tripathi, I. P., & Tiwari, H. L. (2013). Effects of Lead on Environment. *International Journal of Emerging Research in Management & Technology*, 2, 2278–9359.
- Torabi Fard, N., Tadayon, F., Ahmad Panahi, H., & Moniri, E. (2022). Synthesize, characterization and application of a novel three-dimensional magnetic graphene oxide decorated with polyester dendrimers for detection of donepezil hydrochloride in pharmaceutical formulation and biological fluid. *Synthetic Metals*, 290(June), 117141. <https://doi.org/10.1016/j.synthmet.2022.117141>
- Ul-Haq, N., Arain, M. A., Badar, N., Rasheed, M., & Haque, Z. (2011). Drinking water: a major source of lead exposure in Karachi, Pakistan. *Eastern Mediterranean Health Journal*, 17(11), 882–886. <https://doi.org/10.26719/2011.17.11.882>
- Vishwanath, H. S., Shilpa, M. P., Gurumurthy, S. C., Gedda, M., Ramam, K., Eshwarappa, M., Kirana, R., Nath, N., & Mundinamani, S. (2022). Flexible , large-area , multi-layered graphene / cellulose composite for dye filtration applications. *Materials Today Communications*, 30(July 2021), 103134. <https://doi.org/10.1016/j.mtcomm.2022.103134>
- Wang, Q., Zhu, S., Xi, C., & Zhang, F. (2022). A Review: Adsorption and Removal of

- Heavy Metals Based on Polyamide-amines Composites. *Frontiers in Chemistry*, 10(March), 1–15. <https://doi.org/10.3389/fchem.2022.814643>
- Wang, X., Huang, K., Chen, Y., Liu, J., Chen, S., Cao, J., Mei, S., Zhou, Y., & Jing, T. (2018). Preparation of dumbbell manganese dioxide/gelatin composites and their application in the removal of lead and cadmium ions. *Journal of Hazardous Materials*, 350(October 2017), 46–54. <https://doi.org/10.1016/j.jhazmat.2018.02.020>
- Wang, Z., Sim, A., Urban, J. J., & Mi, B. (2018). Removal and Recovery of Heavy Metal Ions by Two-dimensional MoS₂ Nanosheets: Performance and Mechanisms. *Environmental Science and Technology*, 52(17), 9741–9748. <https://doi.org/10.1021/acs.est.8b01705>
- Wang, Z., Tu, Q., Sim, A., Yu, J., Duan, Y., Poon, S., Liu, B., Han, Q., Urban, J. J., Sedlak, D., & Mi, B. (2020). Superselective Removal of Lead from Water by Two-Dimensional MoS₂ Nanosheets and Layer-Stacked Membranes. *Environmental Science and Technology*, 54(19), 12602–12611. <https://doi.org/10.1021/acs.est.0c02651>
- Woehler, S., Bull, T., & Baker, J. R. (2003). *Acetylation of Poly (amidoamine) Dendrimers*. 5526–5529.
- Wuana, R. A., & Okieimen, F. E. (2011). Heavy Metals in Contaminated Soils: A Review of Sources, Chemistry, Risks and Best Available Strategies for Remediation. *ISRN Ecology*, 2011, 1–20. <https://doi.org/10.5402/2011/402647>
- Xu, C., Shi, S., Wang, X., Zhou, H., Wang, L., Zhu, L., Zhang, G., & Xu, D. (2020). Electrospun SiO₂-MgO hybrid fibers for heavy metal removal: Characterization and adsorption study of Pb(II) and Cu(II). *Journal of Hazardous Materials*, 381(Ii), 120974. <https://doi.org/10.1016/j.jhazmat.2019.120974>
- Yan, S., Song, H., Li, Y., Yang, J., Jia, X., Wang, S., & Yang, X. (2022). Applied Catalysis B: Environmental Integrated reduced graphene oxide / polypyrrole hybrid aerogels for simultaneous photocatalytic decontamination and water evaporation. *Applied Catalysis B: Environmental*, 301(October 2021), 120820. <https://doi.org/10.1016/j.apcatb.2021.120820>

- Yang, B., Wei, Y., Liu, Q., Luo, Y., Qiu, S., & Shi, Z. (2019). Polyvinylpyrrolidone functionalized magnetic graphene-based composites for highly efficient removal of lead from wastewater. *Colloids and Surfaces A: Physicochemical and Engineering Aspects*, 582(March), 123927. <https://doi.org/10.1016/j.colsurfa.2019.123927>
- Yosef, M., Fahmy, A., El, W., Hassan, A. M., Khalil, A. S. G., & Anis, B. (2020). High performance graphene-based PVF foam for lead removal from water. *Integrative Medicine Research*, 9(5), 11861–11875. <https://doi.org/10.1016/j.jmrt.2020.08.011>
- You, S., Hu, Y., Liu, X., & Wei, C. (2018). Applied Catalysis B: Environmental Synergetic removal of Pb (II) and dibutyl phthalate mixed pollutants on Bi₂O₃-TiO₂ composite photocatalyst under visible light. *Applied Catalysis B: Environmental*, 232(March), 288–298. <https://doi.org/10.1016/j.apcatb.2018.03.025>
- Zahra, N. (2012). Lead Removal from Water by Low Cost Adsorbents: A Review. *Pakistan Journal of Analytical & Environmental Chemistry*, 13(1), 1–08.
- Zhang, G., Wang, T., Xu, Z., Liu, M., Shen, C., & Meng, Q. (2020). Synthesis of amino-functionalized Ti₃C₂T_xMXene by alkalization-grafting modification for efficient lead adsorption. *Chemical Communications*, 56(76), 11283–11286. <https://doi.org/10.1039/d0cc04265j>
- Zhang, J., Hu, X., Yan, J., Long, L., & Xue, Y. (2020). Crayfish shell biochar modified with magnesium chloride and its effect on lead removal in aqueous solution. 9582–9588.
- Zhang, Y., Zheng, H., Zhang, P., Zheng, X., & Zuo, Q. (2021). A facile method to achieve dopamine polymerization in MOFs pore structure for efficient and selective removal of trace lead (II) ions from drinking water. *Journal of Hazardous Materials*, 408(August 2020), 1–10. <https://doi.org/10.1016/j.jhazmat.2020.124917>
- Zhao, W., Zhu, G., Daugulis, A. J., Chen, Q., Ma, H., Zheng, P., Liang, J., & Ma, X. (2020). Removal and biomineralization of Pb²⁺ in water by fungus *Phanerochaete chrysosporium*. *Journal of Cleaner Production*, 260, 120980.

<https://doi.org/10.1016/j.jclepro.2020.120980>

Zinatloo-ajabshir, S., Sadat, M., Amiri, O., & Salavati-niasari, M. (2020). Green synthesis of dysprosium stannate nanoparticles using *Ficus carica* extract as photocatalyst for the degradation of organic pollutants under visible irradiation. *Ceramics International*, 46(5), 6095–6107. <https://doi.org/10.1016/j.ceramint.2019.11.072>